**TECHNISCHE MECHANIK**
an open access journal

journal homepage: www.ovgu.de/techmech

Tech. Mech., Vol. 45, Is. 1, (2025), 88–109

Received: 11.04.2025
Accepted: 24.09.2025
Available online: 09.10.2025

# 3D comparative study of the thermodynamics of fluid flow and an analysis of heat transfer by convection in different flat air solar collectors

Fayssal Benosman, and Mohammed Amine Amraoui *

University Djillali LIABES Sidi-Bel-Abbès, Faculty of Technology, Department of Mechanical Engineering, , BP 89 22000 Sidi-BelAbbès, Algeria

**Abstract:** The article shows a 3D analysis using CFD (computer simulation software) software that resolves turbulent flow in the three types of devices for increasing air temperature which are named collector works by sun with transverse obstacles and small circular obstacle (SCTBSC), collector works by sun with different lengths of transverse baffles (SCDLTB) and Solar collector with transverse baffles (SCTB). This comparative study analyzes the thermodynamic behavior in air streams equipped with different baffles. The effect of reducing the flow passage surface caused by the baffles will increase the airspeed by 832%, 850%, and 1552% compared to the inlet speed for (SCTBSC), (SCDLTB) and (SCTB), respectively.

**Keywords:** aerodynamics, turbulence, thermodynamics, fluid mechanics and CFD

## 1 Introduction

Due to insufficient temperature increase carried out in air heaters by the sun, it is relevant to consider improvements to optimize performance or increase thermal efficiency. Thus, many researchers have undertaken research aimed at improving the quality of convection between the absorber and the air, with the aim of convection in devices that heat the air in devices that heat air.

Karim and Amin (2015) performed simulations on various types of solar heaters, observation of fluid displacement characteristic on the quality of the convection temperature change of the collector. The authors observed that the solar collector model equipped with a V-shaped double-pass absorber offers superior superior temperature absorption qualities. Bouzaher et al. (2019) created a tube with rigid obstacles. They observed that the fluid disorder created by these obstacles routed to an improvement of the thermal convection at the level of of fluid movement in the collector. The researchers also examined the impact of bulk fluid flow on the thermodynamics of flow inside the heater. The research of Benosman and Amraoui (2021) presented an in-depth analysis of an inclined obstacle air heater by analyzing the fluid characteristics through the study of physical dimensions or unit analysis. Using the commercial CFD software ANSYS Fluent, Cagnoli et al. (2017) performed a computer analysis concerning the temperature covection in the heater, as well as the radiations of temperature transfer by the enclosed facades of the latter. By comparing the absorption and the access of the collector, they evaluated the energy losses to the outside. These results were performed on a single air flow to obtain an analysis of the impact of the geometry and the displacement of the mass fluid on the thermal qualities of the receiver.

Researchers Menni et al. (2021) learned a thermodynamic analysis of two sun channels equipped with arc-shaped deflectors, one curved forward and the other curved backward, allowing them to obtain different consequences on Dimensional quantities are particularly involved in fluid mechanics and presentation of speed and temperature fields. Amraoui and Aliane (2014a) work et al consisted of a 3D simulation for increasing air temperature equipped with transverse and longitudinal deflectors, using ANSYS software they provided several results on the change in air convection and their physical characteristics, they concluded that the baffles increase the flow path as well as the turbulence which gives better thermal efficiency for the solar collector. A computer demonstration was made by Abdi et al. (2022). of an air heater equipped with baffles in the form of wings. The effect of these baffles eliminated dead zones and unwanted recirculation, They concluded that the increase in the dimensionless Reynolds magnitude is associated with an increase in the dimensionless Nusselt magnitude, the researchers made a correlation between the sliding force and the holding force produced at the contact of two surfaces and analyzed Dimensionless quantities are particularly involved in fluid mechanics. The research by Diarce et al. (2014) proposes a 2D numerical study by computer software. They conducted a computational analysis to design a climate-controlled wall incorporating a material capable of changing its physical state in a temperature range (PCM) in its wall thickness from the outside. The information from the study was compared with practical data collected using a large-scale PASLINK test platform. They also assimilated the different models given by the calculation software to simulate the characteristics of the fluid at the zone that has the temperature change.

A computer investigation of a collector operating under the sun equipped with transverse obstacles that do not touch the absorber was achieved by Amraoui and Aliane (2014b). Comparison between their numerical solutions and experimental data revealed a good correspondence between the two. They provided various results regarding the distribution of velocity, temperature and turbulence. Air channels are used to cool and heat homes or dry food products such as solar collectors. Improving their thermal

* E-mail address: amraoui_mohammedamine@yahoo.fr doi: 10.24352/UB.OVGU-2025-043 

efficiency has been and remains a major concern for theorists and practitioners. Menni et al. (2019a) proposed a set of knowledge regarding the thermal domain works, they made an in-depth study on different research of the improvement of fluid thermodynamics. A computational analysis of the heat collector was performed by Khaldi et al. (2017b). They found that adding storage systems can improve the mass flux by 32% during the night. Applying a bed of packing material can reduce the heat variations of the crops by up to 76%, thus adding the period of the air heater running by waiting for 12.5 hours. By extending the porousness from 0.1 to 0.8, the maximum temperature can be increased by about 10°C. This is part of the optimization of heat exchange in solar air heaters.

Amraoui (2021a) Conducted a comparative study on a device for heating air with the sun fitted with transverse baffles with a single pass and a heating device fitted with transverse obstacles with a double pass, He drew several conclusions indicating that the second model offers better thermal performance. compared to the first solar collector. Using 3D digital simulation using the ANSYS calculation code, Amraoui and Aliane (2018) presented work on airflow in an airplane solar collector, he created transverse baffles which occupied 80% of the width of the heat device to increase the exchange surface and to eliminate dead zones by adding small baffles between the transverse baffles, they observed several results on the thermodynamics of the air in the air stream of a fluid heater. In the field of simulation of an incompressible fluid in a solar channel,Menni et al. (2019b) studied the fluid displacement in an air vein equipped with baffles in the form of S, the aerothermal results are given by the CFD FLUENT, they presented the results on the energy change and the physical properties of the fluid such as the dimensionless Nusselt number and presented the relationship through the sliding capacity and the holding capacity produced at the contact of two surfaces. To increase the Trouble in the collector works by sun Amraoui and Benosman (2021) added square baffles which gave high efficiency through computer calculation by CFD ANSYS, they gave equations governing the air movement and their thermal characteristic in the air flow they concluded results on the thermodynamics of the incompressible fluid.

For the manufacture of houses with thermal comfort and energy saving, Villi et al. (2009) investigated roofs designed to cool homes, using CFD software to establish correlations to characterize the phenomena of air movement and thermal change in the air change zones, application over a full year. A CFD simulation with the computer software STAR-CCM+ was performed by Zilio et al. (2017) to understand the origin of the source of the power emitted by the fuel oil in the basins of a navigator. They considered the influence of various soil and flight requirements. The aluminum at the level of the basin wing was studied, taking into account the leading edge effects, the change in fluid displacement (fluid fuel) through the various cells of the basin, as well as the air movement in the cavity. The article of Amraoui et al. (2023) was to improve explanations on the development of thermal convection in heating devices, they simulated a solar collector with two flow voices, this type of collector gives a large heat exchange surface, and this study could inspire new research in the area of increasing thermal efficiency in air-plane solar collectors. Amraoui (2011) carried out a comparative study between Various collectors for heating the air by the sun (flat solar air heater equipped only with baffles, with baffles and rectangular roughness and the other triangular roughness and the last circular roughness). he deduced conclusions on energy transfer in the sun channels with the addition of roughnesses of different shapes at the level of the insulation, thus concluding that the solar collector with rectangular roughness gives better performance compared to other models. To improve heat transfer in air-plane solar collectors Amraoui (2021b) added circular obstacles to to the air channel of the solar heater to increase turbulence, using ANSYS software, he made 3D simulations of the collector solar obtaining several results that show the improvement of change by convection thanks to circular obstacles.

Among the heat transfer problems of solar energy application is poor convection in fluid flow therefore Aliane and Amraoui (2013) created triangular roughness at the air moving part provided with the obstacles to increase turbulence in order to improve the operation of the device that heats the air. A 2D numerical study of a device for heating fluid by sun was created by Khaldi et al. (2017a), where they created another air inlet for the sun air heater model to obtain a more homogeneous temperature distribution. The researchers used the environment of Tlemcen for a day in August to analyze. Aoues et al. (2009) made a real analysis of different dryers for heating air equipped with a promoter to increase turbulence. Placed in the Biskra area, the collectors were mounted towards the south. The authors compared several models in order to give the best type which offers excellent convection. Bahria and Amirat (2013) favored the analysis of the effect of obstacles on the increase of the energy change in the air movement towards the collector to increase the air temperature provided with Labyrinth and longitudinal obstacles provided under the plate that absorbs heat. The authors showed the famous theorem of Hottel et al. to simulate the devices to heat the fluid by sun. They obtained that the obstacles give a significant turbulence, the latter increases the thermal convection by the displacement of the fluid. Bourdeau et al. (1980) used phase change materials for space heating, they built a diode wall using one-way air circulation between the front face and the isolated rear volume, it is a kinetic study of the thermal transfers at the storage level. This study concerns a mathematical modeling of a two-pass solar air collector.

Zerrouki et al. (2002) presented an exact mathematical solution of the two-pass solar collector. They provided the exact expressions for the thermal conductance coefficient and the total conductance of a steady-state two-pass solar collector. These expressions are not yet available in the literature. Comparison of the results with those obtained with the Bliss - Whillier analysis is satisfactory. Researchers Mokhtari and Semmar (1999) gave a real work of a solar air collector. The results presented in this document allow us to draw important conclusions as follows. The fluid outlet temperature varies depending on the solar flux. This design made it possible to obtain fairly high fluid temperatures at the outlet, favorable for using them in the drying of food products. These experimental results aided in a possible theoretical analysis of the experimental system. Forward losses are difficult to estimate due to the difficulty of the problems occurring in this part of the collector. The study of Benkhelifa (1998) allowed him to find a mathematical model that calculates the thermal losses towards the front of a flat solar collector, he exploited the program to learn the influence of some characteristics on the coefficient of energy losses towards the

front of the UL collector. Examining the results, he noticed that the UL index goes increasing with the growth of the emissivity of the absorber Ep, the temperature of the absorbing plate Tp and the coefficient of convective exchange with the ambient air hc,a .

The objective of the work of Semmar et al. (1998) was the study and design of an air solar collector based on a model selected among others. A comparative study between the performance parameters characterizing the theoretical model and those presented by the test bench was carried out. They also noted that in the case of forced convection, they have a significant flow of hot air in flow rates of the outlet temperature which is lower than that obtained for natural convection where the flow is interior to the first. What they were able to conclude at the end of this process was that the difference recorded between the calculated results and those measured was not considerable. Among the studies that aim to increase the capacity of an energy recuperator in solar collectors, we find the study of Amraoui and Aliane (2015) who installed longitudinal and transverse obstacles to enlarge the useful surface of an exchanger in the area of the fluid used and increase the turbulence to improve the capacity of an energy recuperator of the collector.

Regarding this study, we will approach a 3D aerodynamic and thermal study with the intention of present the nature of the displacement by action of obstacles on the thermodynamic behavior of the displacement in the air blade in the three types of sun air heating devices. (SCTBSC), (SCDLTB) and (SCTB).

## 2 Problem

CFD can be used to model complex flows and study the behavior of fluids near baffles. CFD can provide detailed information on the velocity field, heat transfer, and flow phenomena around collectors, which can influence their performance. Simulation can reveal interaction effects between multiple collectors and variations in performance depending on different geometric configurations.
In our study, we modeled three forms of flat solar air heaters (solar air heater with transverse obstacles and small circular baffles (SCTBSC), solar collector with transverse baffles of variable lengths (SCDLTB), and solar collector with transverse baffles (SCTB)) shown in Figure 1. The sizes of these collectors, namely length L=0.9, width W=0.5 and height Y=0.025. The absorber at a temperature (Tab=380k), the temperature of the insulator ($T_{iso}$ = 340), the inlet temperature ($T_0 = 300k$), the initial speed ($U_0$) and the outlet pressure ($P = P_{atm}$).
The use of ANSYS CFD software allowed to conduct a three-dimensional analysis. The selected turbulence model is the $k-\varepsilon$, $k = 0.005 \times U_0^2$, $\varepsilon = 0.1 \times k^2$. The Reynolds numbers are between 60,000 and 200,000.

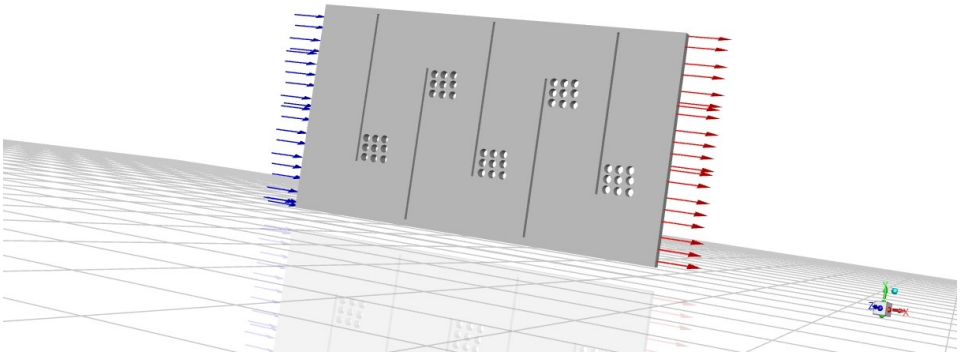

(A)

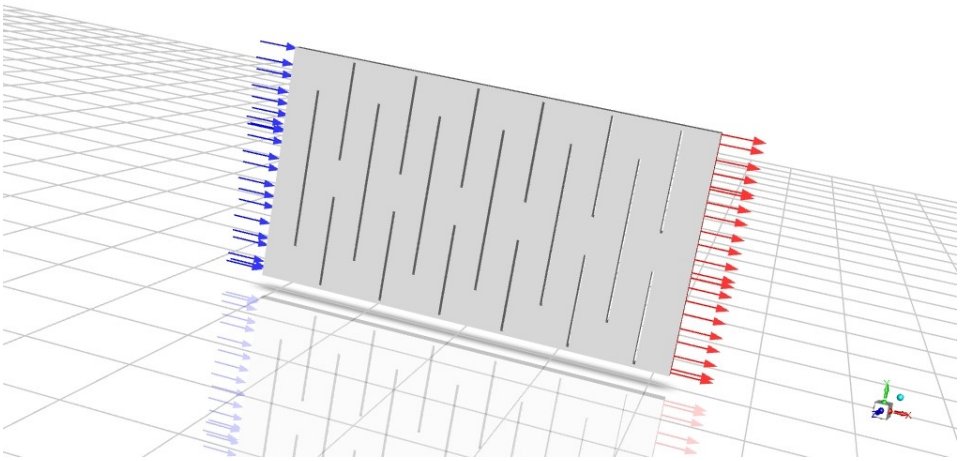

(B)

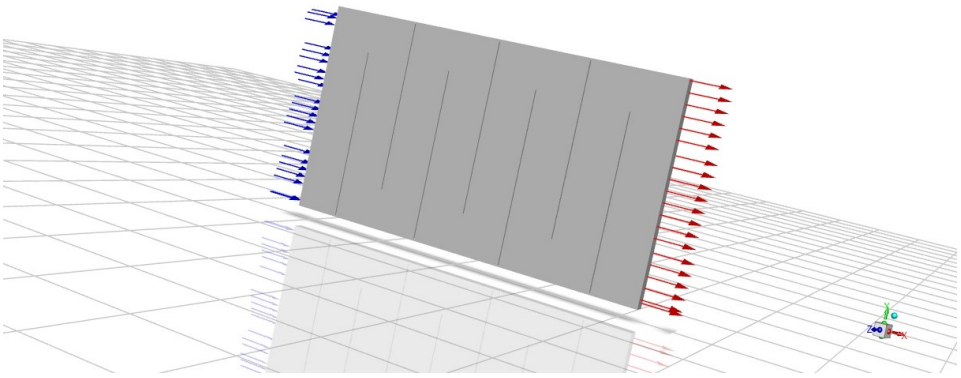

(C)

Fig. 1: Solar air heater with transverse obstacles and small circular obstacle (SCTBSC) (A), air dryer with different lengths of transverse baffles (SCDLTB) (B), and Solar collector with transverse baffles (SCTB) (D)

## 3 Controlling equations

1. The first equation:
   In fluid mechanics, the basis of conservation of mass can be described by the law of continuity

$$\nabla \cdot \left(\rho \overrightarrow{v}\right) = 0 \tag{1}$$

$$\frac{\partial}{\partial x}\left(\rho v_x\right) + \frac{\partial}{\partial y}\left(\rho v_r\right) + \frac{\rho v_r}{r} \tag{2}$$

2. Second equation:
   Momentum conservation is represented by

$$\nabla \cdot \left(\rho \overrightarrow{v}\,\overrightarrow{v}\right) = -\nabla p + \nabla\left(\overline{\overline{\tau}}\right) + \rho \overrightarrow{g} \tag{3}$$

$$\overline{\overline{\tau}} = \mu\left[\left(\nabla \overrightarrow{v} + \nabla \overrightarrow{v}^{T}\right) - \frac{2}{3}\nabla \cdot \overrightarrow{v} I\right] \tag{4}$$

   The right side represents the action of volume development
   The equations for conservation of the two direction are expressed by:

$$\frac{1}{r}\frac{\partial}{\partial x}\left(r\rho v_x v_x\right) + \frac{1}{r}\frac{\partial}{\partial r}\left(r\rho v_r v_x\right) = -\frac{\partial p}{\partial x} + \frac{1}{r}\frac{1}{r}\frac{\partial}{\partial x}\left[r\mu\left(2\frac{\partial v_x}{\partial x} - \frac{2}{3}\left(\nabla \cdot \overrightarrow{v}\right)\right)\right] + \frac{1}{r}\frac{\partial}{\partial r}\left[r\mu\left(\frac{\partial v_x}{\partial r} + \frac{\partial v_r}{\partial x}\right)\right] \tag{5}$$

$$\frac{1}{r}\frac{\partial}{\partial x}\left(r\rho v_x v_r\right) + \frac{1}{r}\frac{\partial}{\partial r}\left(r\rho v_r v_r\right) = -\frac{\partial p}{\partial r} + \frac{1}{r}\frac{\partial}{\partial x}\left[r\mu\left(\frac{\partial v_r}{\partial x} + \frac{\partial v_x}{\partial r}\right)\right] + \frac{1}{r}\frac{\partial}{\partial r}\left[r\mu\left(2\frac{\partial v_r}{\partial r} - \frac{2}{3}\left(\nabla \cdot \overrightarrow{v}\right)\right)\right] - 2\mu\frac{v_r}{r^2} + \frac{2}{3}\frac{\mu}{r}\left(\nabla . \overrightarrow{v}\right) + \rho\frac{v_z^2}{r} \tag{6}$$

   where, $\nabla \cdot \overrightarrow{v} = \frac{\partial v_x}{\partial x} + \frac{\partial v_r}{\partial r}\frac{v_r}{r}$ and $v_z$ is the swirl velocity.

$$\frac{1}{r}\frac{\partial}{\partial x}(r\rho u w) + \frac{1}{r}\frac{\partial}{\partial r}(r\rho v w) = \frac{1}{r}\frac{\partial}{\partial x}\left[r\mu\frac{\partial w}{\partial x}\right] + \frac{1}{r^2}\frac{\partial}{\partial r}\left[r^3\mu\frac{\partial}{\partial r}\left(\frac{w}{r}\right)\right] - \rho\frac{v w}{r} \tag{7}$$

   The Energy Equation:

$$\nabla \cdot \left(\overrightarrow{v}\left(\rho E + p\right)\right) = \nabla \cdot \left(k_{eff}.\nabla T - \sum_j h_j \cdot \overrightarrow{j}_j + \left(\overline{\overline{\tau}}_{eff} \cdot \overrightarrow{v}\right)\right) \tag{8}$$

the right side presents the different energy transmission.

$$k_{eff} = k' + \frac{c_p \mu_t}{\mathrm{Pr}_t} \tag{9}$$

$Pr = 0.85$

$$E = h' - \frac{p}{\rho} + \frac{v^2}{2} \tag{10}$$

$$h' = \sum_j Y_j h_j + \frac{p}{\rho} \tag{11}$$

$$h_j = \int_{T_{ref}}^{T} c_{p.j} dT \tag{12}$$

where $T_{ref} = 298.15K$.

The standard k-$\varepsilon$ turbulence model:

This is a two-equation model that has been the most widely tested and used, the good description of external flows around obstacles has been developed for a long time, converges very quickly, can also be developed directly on equations of statistical moments at a point, this is how the k-$\varepsilon$ model was originally introduced, this type generally gives better solution in simple displacements but cannot satisfactorily reproduce the characteristics of complex flows, Difficulties have also arisen for relatively simple turbulent flows. has become the most popular of the turbulence models for its simplicity and the possibility of using it for different types of flows.

We chose to use the k-$\varepsilon$ turbulence model in our study because it is generally based on the wall law approach. However, as Wilcox (1993) pointed out, this model has accuracy limitations in the regions close to the walls. To ensure correct modeling, the first mesh point must be located in the logarithmic region of the boundary layer, i.e., for a value of $y^+ \approx 30$. One of the main advantages of this approach is that it avoids the need for a highly refined mesh in the vicinity of solid walls.

Our choice of the k-$\varepsilon$ model is also supported by the results of our previous study (Amraoui and Aliane (2014b) and Amraoui and Aliane (2018)), in which a comparison between experimental data (from the work of Abdelhafid (1994) and Slama (2007)) and numerical simulations based on the k-$\varepsilon$ model was carried out. This comparison showed good agreement of the collector outlet temperatures for different flow velocities, as illustrated in Figure 4 and Table 2. These results thus validate the relevance of using the k-$\varepsilon$ model in our current study.

$$\frac{\partial}{\partial x_i}(\rho k u_i) = \frac{\partial}{\partial x_j}\left[\left(\mu + \frac{\mu_t}{\sigma_k}\right)\frac{\partial k}{\partial x_j}\right] + G_k - \rho_\varepsilon \tag{13}$$

$$\frac{\partial}{\partial x_i}(\rho \varepsilon u_i) = \frac{\partial}{\partial x_j}\left[\left(\mu + \frac{\mu_t}{\sigma_\varepsilon}\right)\frac{\partial \varepsilon}{\partial x_j}\right] + C_{1\varepsilon}\frac{\varepsilon}{k}G_k - C_{2\varepsilon}\rho\frac{\varepsilon^2}{K} \tag{14}$$

$$G_k = -\rho\overline{u_i' u_j'}\frac{\partial u_j}{\partial x_i} \tag{15}$$

3. The third equation:
   The relation of $\mu_t$ is presented by:

$$\mu_t = \rho \cdot C_\mu \frac{k^2}{\varepsilon} \tag{16}$$

where $C_\mu$ is a constant $C_{1\varepsilon} = 1.44$, $C_{2\varepsilon} = 1.92$ , $C_\mu = 0.99$, $\sigma_k = 1.0$, $\sigma_\varepsilon = 1.3$ .

## 4 Results and explanation

### 4.1 Mesh

We used the non-uniform mesh shown in Figure 2.

Tab. 1: The mesh characteristics of the four configurations of solar air dryers

| Model | (SCTBSC) | (SCDLTB) | (SCTB) |
|---|---|---|---|
| Order elements | linear | linear | linear |
| Export format | Standard | Standard | Standard |
| Mesh | Simple | Simple | Simple |
| The smoothing | Average | Average | Average |
| Inflation option | Gradual transition | progressive transition | progressive transition |
| The number of elements | 157155 | 164565 | 299584 |
| The number of nodes | 182608 | 141106 | 329934 |

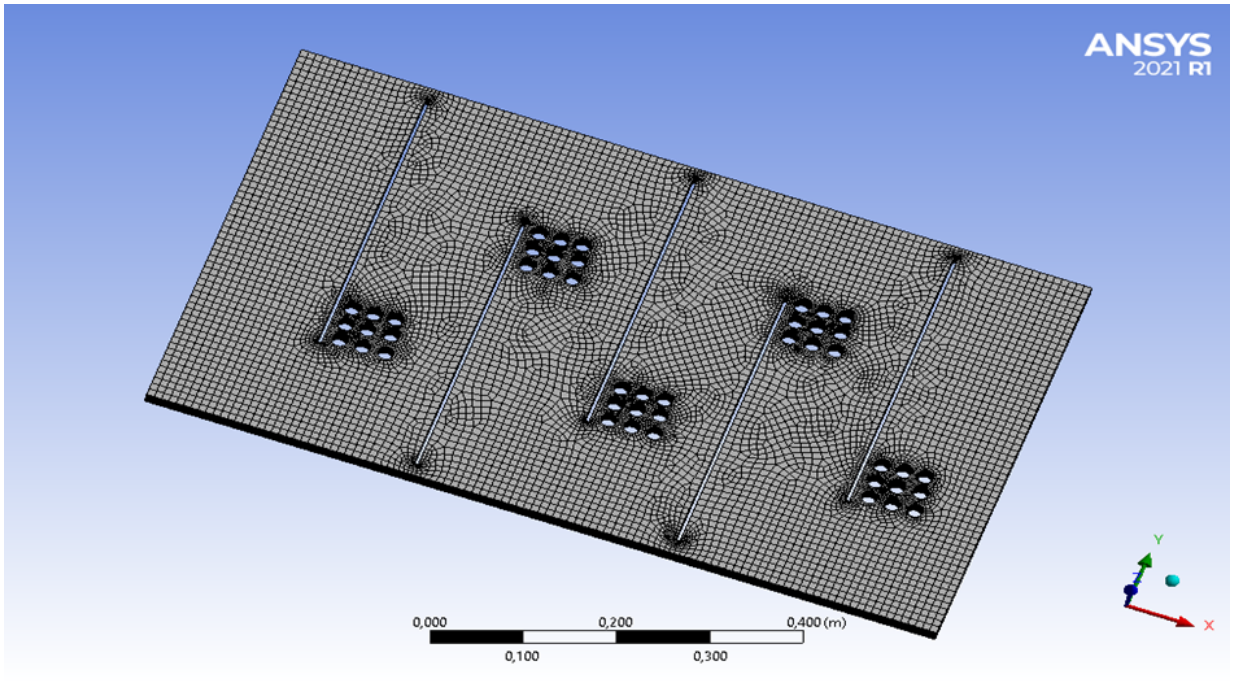


(A)

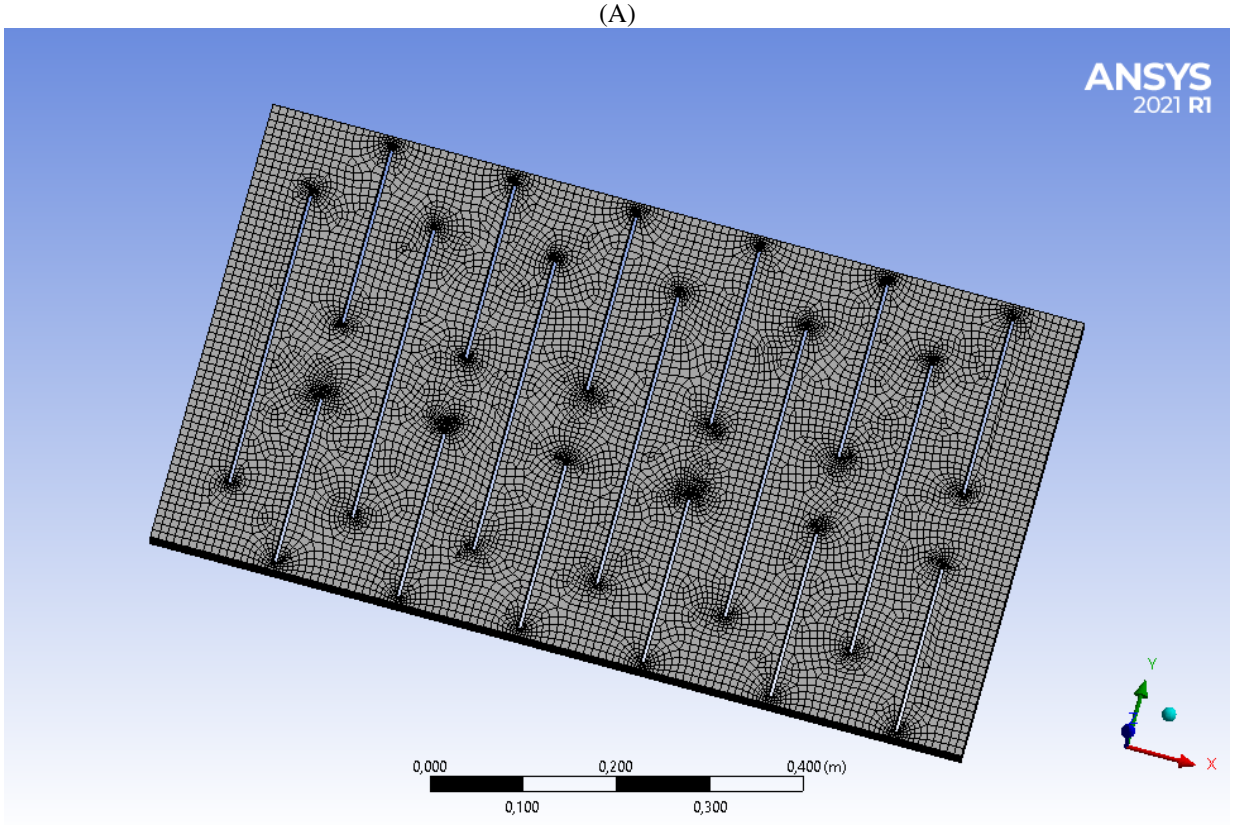


(B)

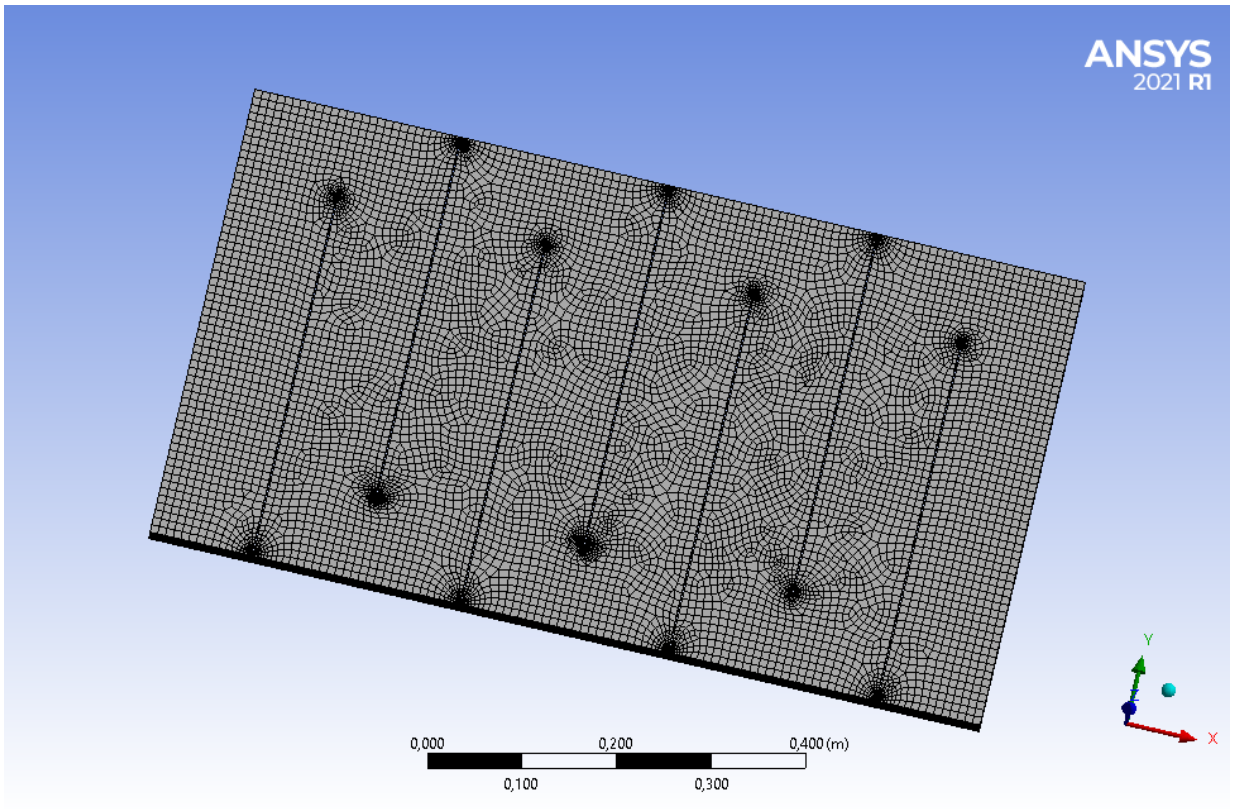


(C)

Fig. 2: Collector mesh of type (SCTBSC) (A), type (SCDLTB) (B) and type (SCTB) (C)

Mesh independence is an important concept in numerical analysis. It refers to the property that the numerical solution to a problem does not depend on the size or shape of the mesh used to discretize the domain. In other words, if the mesh resolution is increased by reducing the mesh size, the numerical solution should converge towards the exact solution of the problem, regardless of how the mesh is constructed. This notion is fundamental to ensure the accuracy and reliability of numerical simulations. We verified the mesh independence presented in Figure 3 during the analysis of the results obtained by performing convergence studies in which we compare the solutions for different meshes. This ensures that the results are not influenced by arbitrary mesh choices, but rather accurately reflect the behavior of the modeled system.

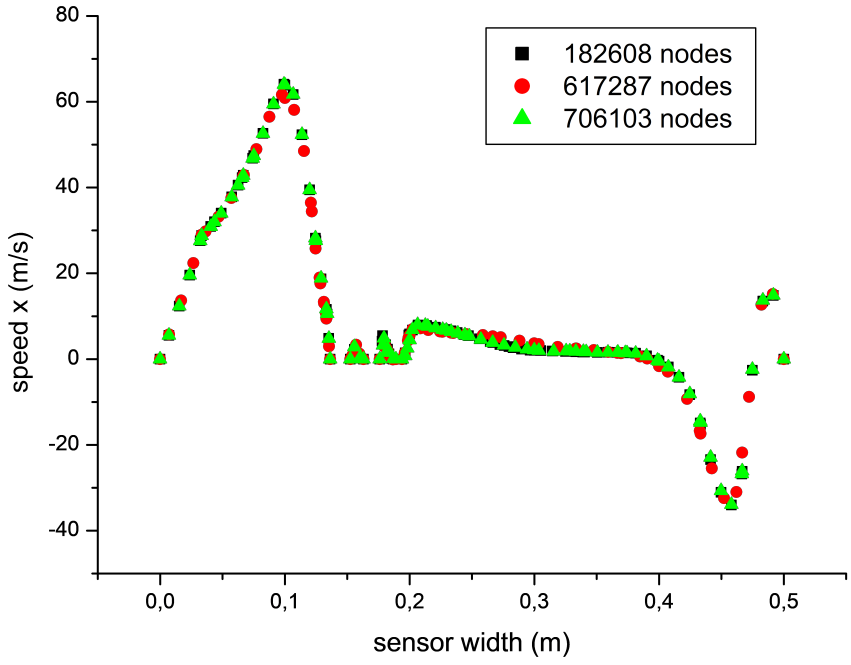


(A)

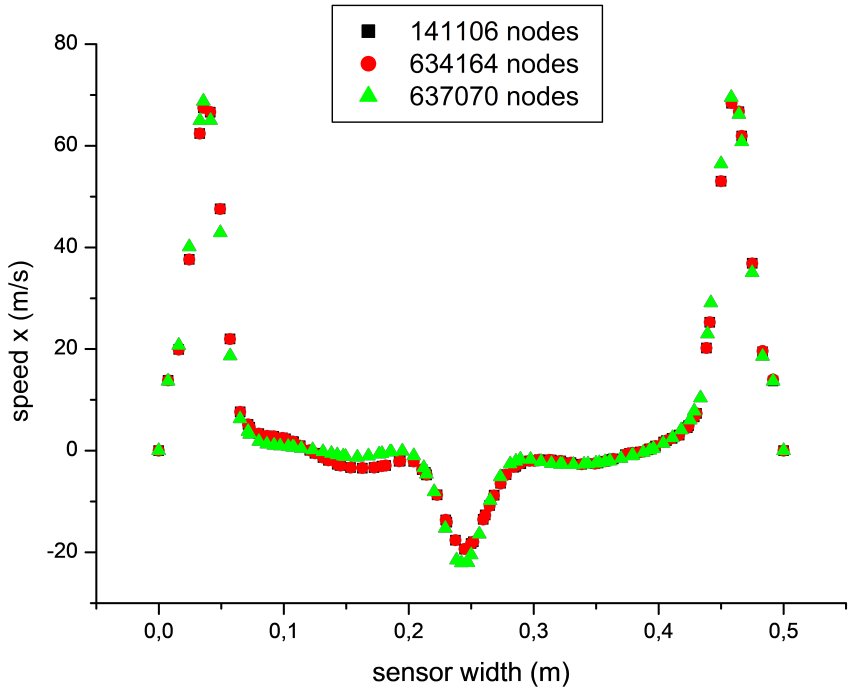


(B)

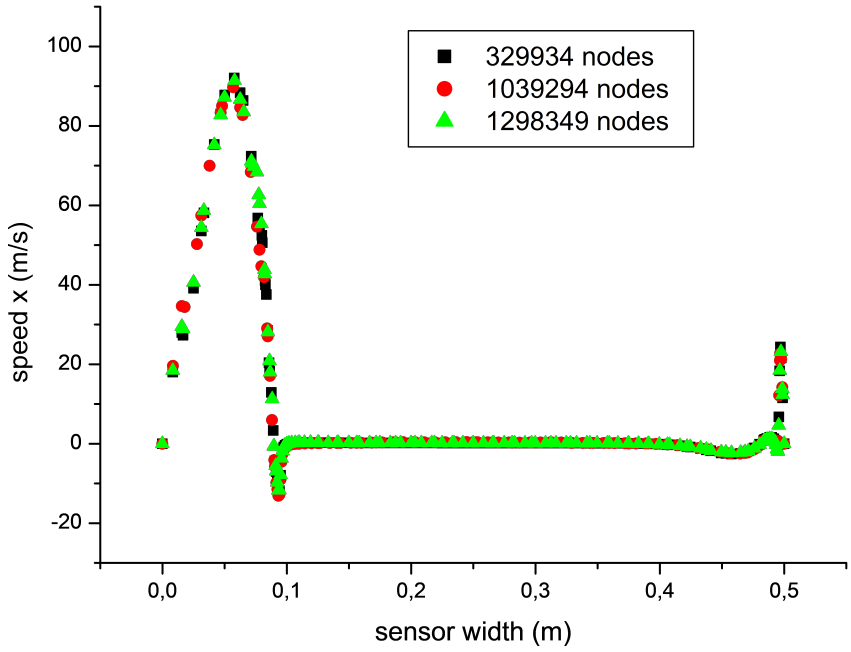


(C)

Fig. 3: axial velocity profiles for different nodes of type (SCTBSC) (A), type (SCDLTB) (B) and type (SCTB) (C)

### 4.2 Validation

Our computer analysis MA Amraoui and Aliane (2018) is evaluated by the real study M Abdelhafid (1994), we have noticed that there is a good agreement for the two results see figure 4.
Table 2 presents the validation of our numerical work and the experimental work of Amraoui and Benosman (2021).

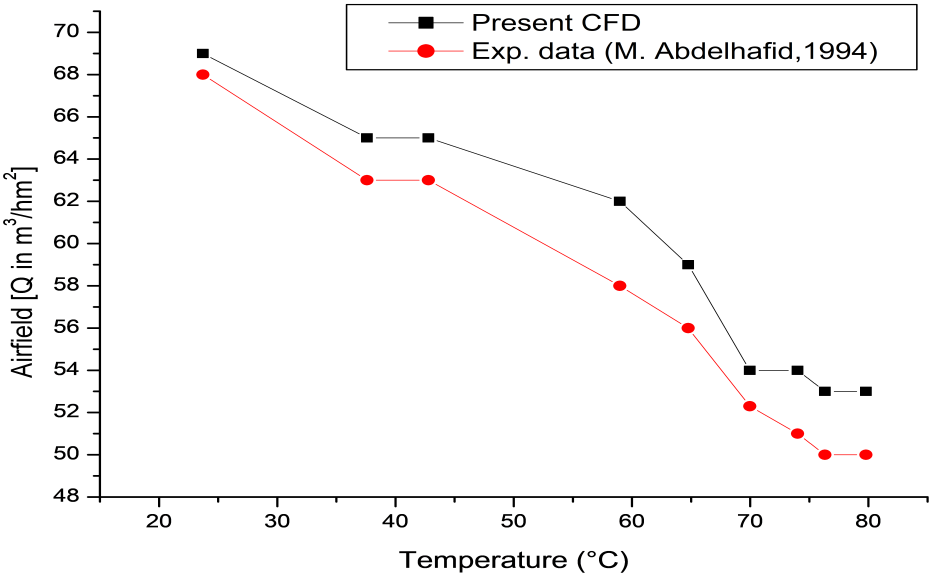


Fig. 4: Evaluate the simulation results with the real data published in reference Amraoui and Aliane (2018)

Tab. 2: Validation of CFD results by experimental results (Amraoui and Aliane (2014b))

| Flow ($m^3/hm^2$) | Collector $\Delta T$ by CFD (°C) | Collector $\Delta T$ (°C) Slama (2007) |
|---|---|---|
| Q1=50 | 33 | 30.51 |
| Q2=35 | 51 | 52.60 |

### 4.3 Findings and analysis

Figure 5 illustrates the velocity distribution in the air ducts of the three air solar heaters. For the first model, transverse baffles are present to lengthen the flow path, thus increasing the heat exchange surface, while small circular baffles are added to sweep the fixed air parts created by the transverse obstacles. The velocity around the baffles amounts to 832% compared to the inlet velocity. For the second model, the flat air solar heater incorporates transverse baffles of different lengths, arranged to create a double passage, thus extending the flow path. We observed that the velocity is significantly higher at the outlet of the baffles, reaching an increase of 850% compared to the inlet velocity. The third model is equipped with transverse baffles that increase the air velocity and improve convection. It was also found that the velocity near the obstacles increases to 1552% comparing by the initial velocity.

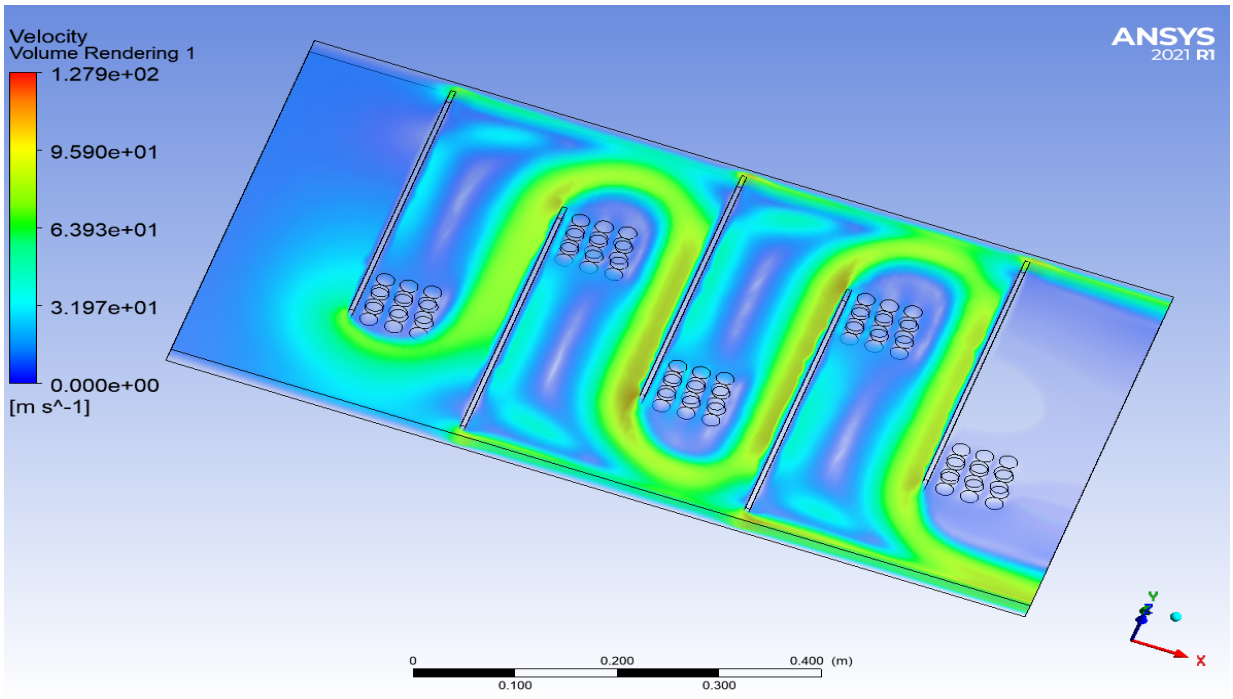


(A)

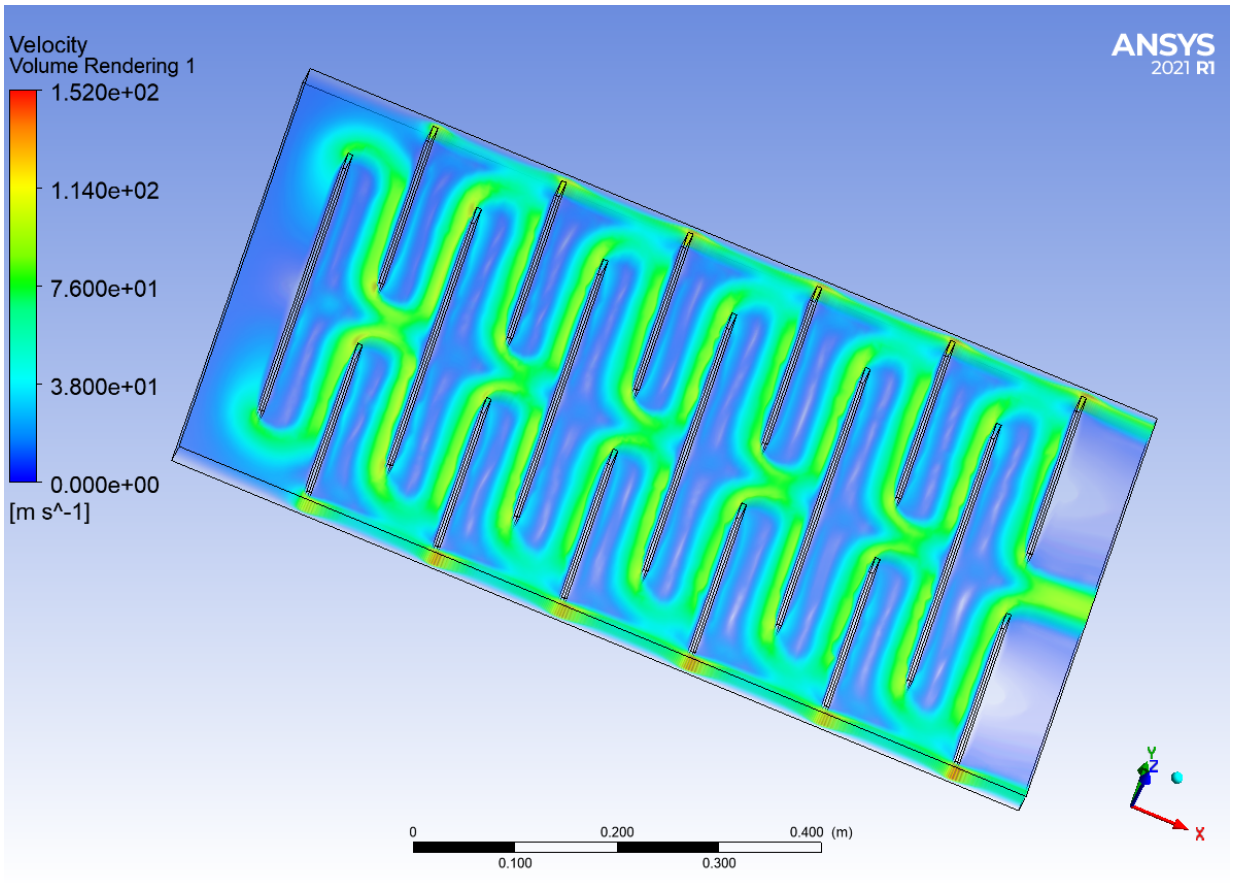


(B)

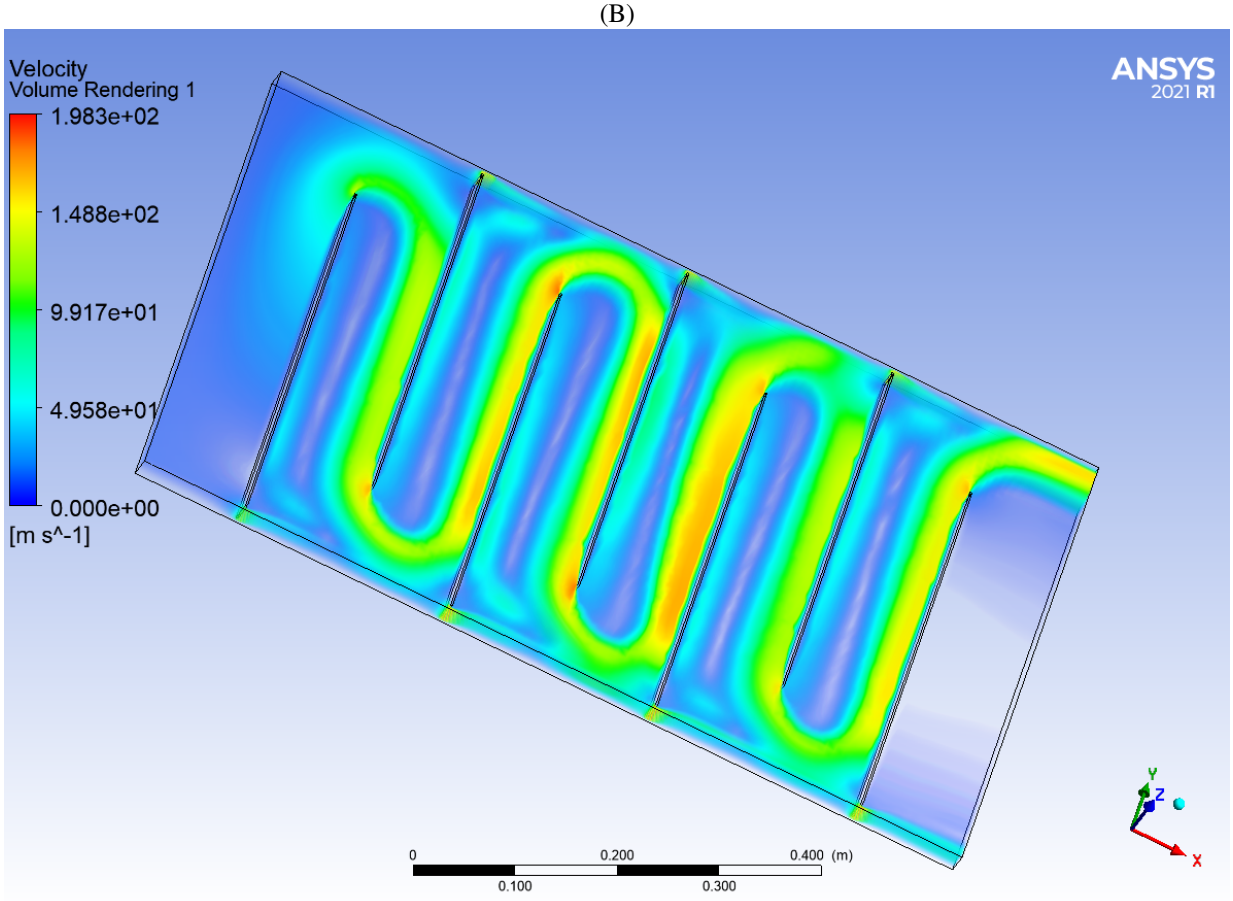


(C)

Fig. 5: Speed presentation in model (SCTBSC) (A), model (SCDLTB) (B) and model (SCTB) (C) for : $V_e = 12m/s$

Figure 6 shows the velocity profile during air movement over all three models studied, revealing lower velocities away from the baffles and higher velocities near them.

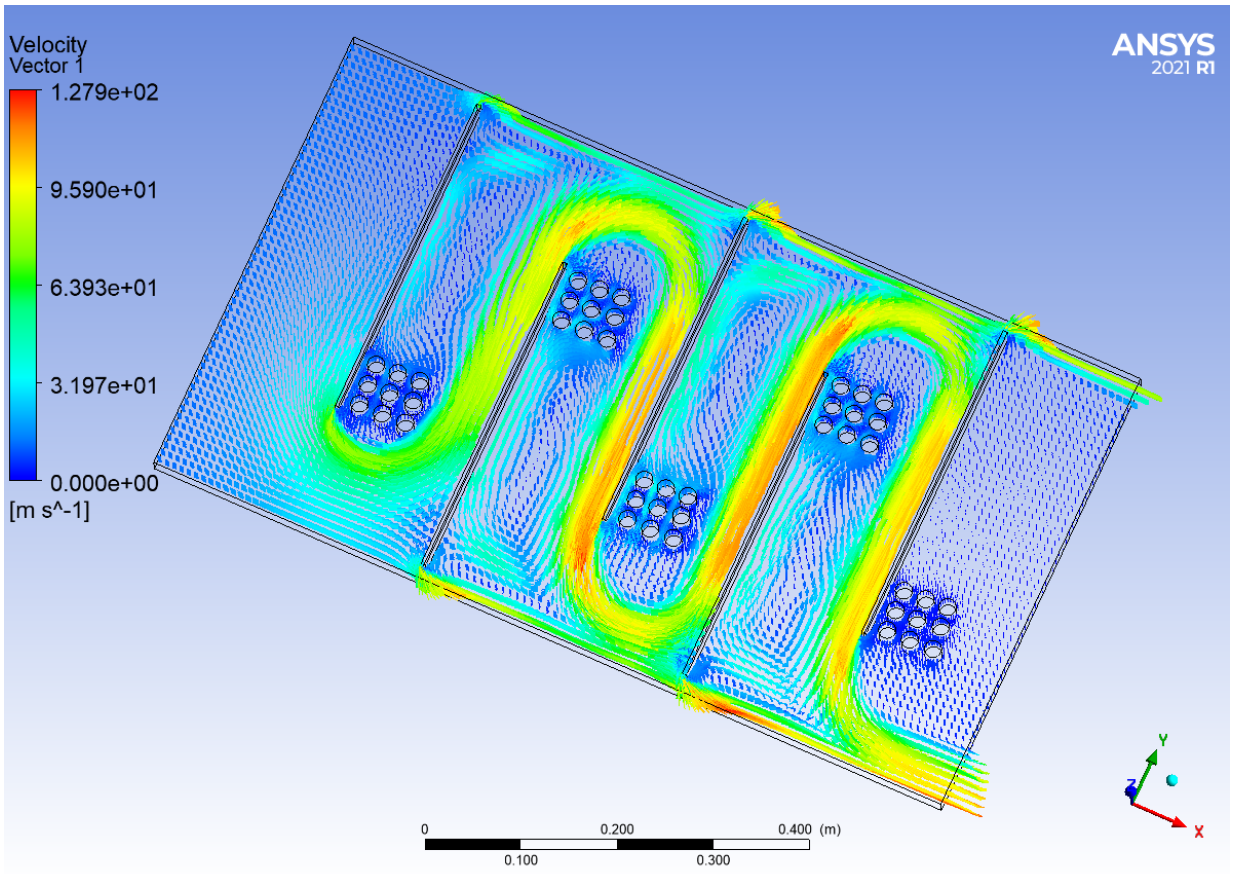
Velocity
Vector 1
1.279e+02
9.590e+01
6.393e+01
3.197e+01
0.000e+00
[m s^-1]
ANSYS
2021 R1
0
0.200
0.400 (m)
0.100
0.300
Y
Z
X

(A)

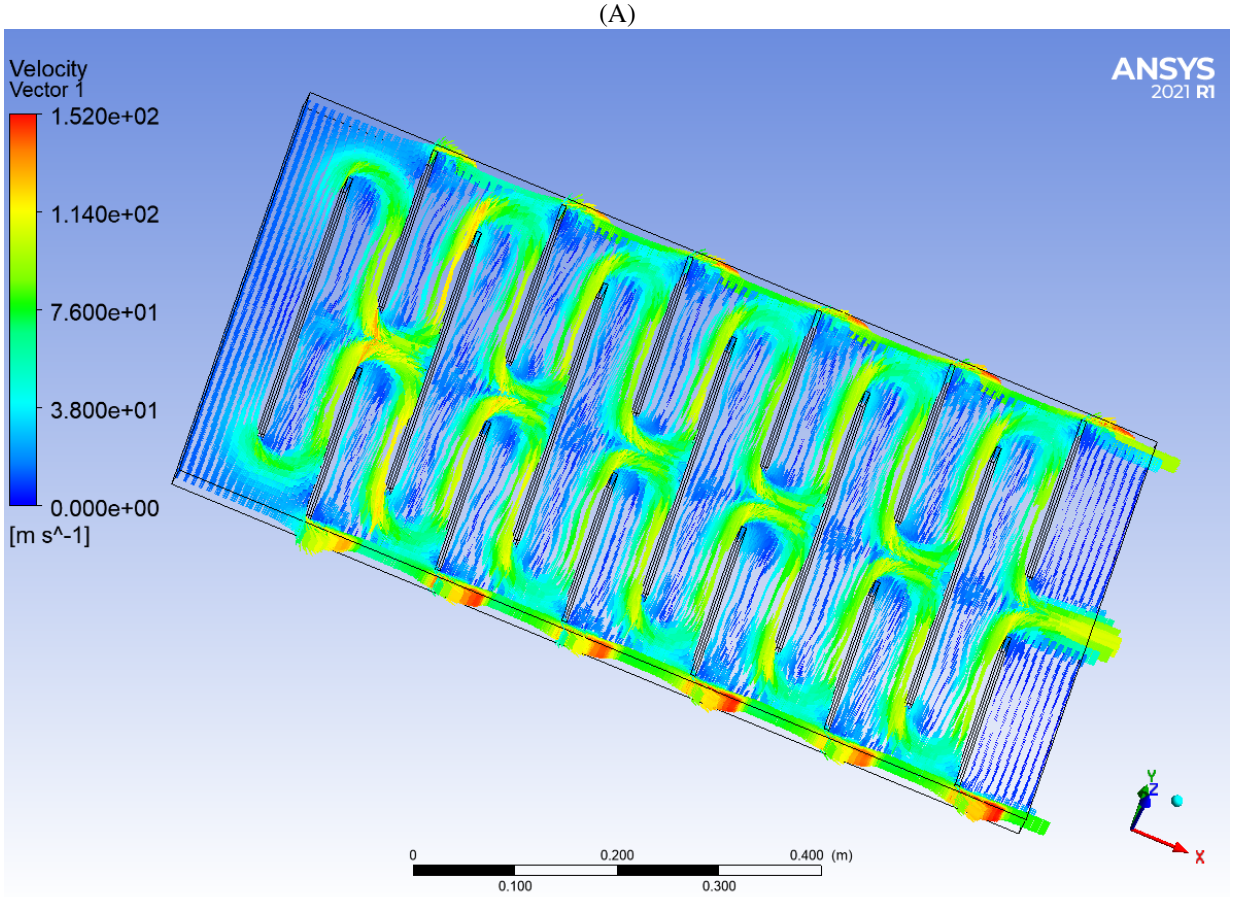
Velocity
Vector 1
1.520e+02
1.140e+02
7.600e+01
3.800e+01
0.000e+00
[m s^-1]
ANSYS
2021 R1
0
0.200
0.400 (m)
0.100
0.300
Y
Z
X

(B)

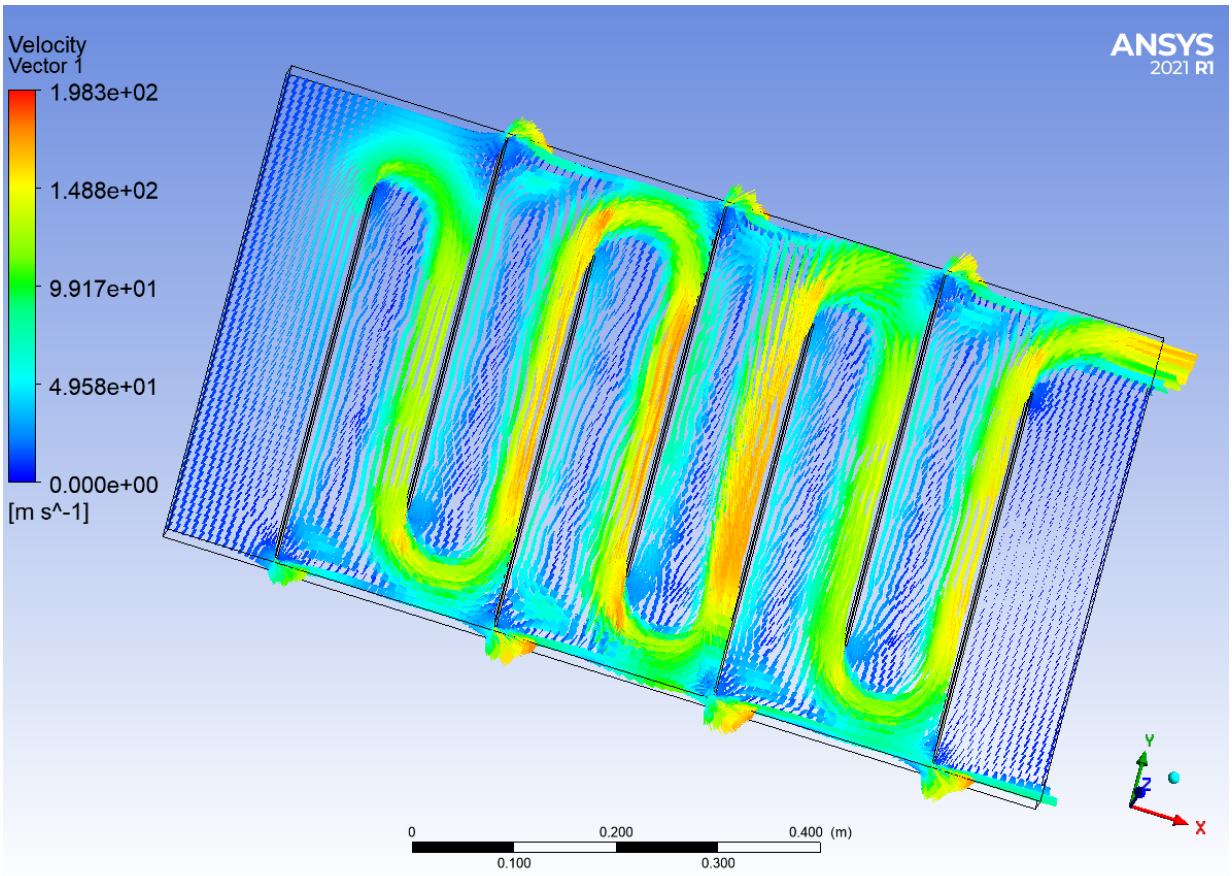


(C)

Fig. 6: Vector presentation in model (SCTBSC) (A), model (SCDLTB) (B) and model (SCTB) (C) for : $V_e = 12m/s$

The boundary layer is the thin region located near the walls and baffles of solar collectors where the effects of viscosity are significant. Within the boundary layer, we also identify a thermal boundary layer, in which the temperature of the fluid gradually evolves between the temperature of the solid surface and that of the fluid located far from this surface. We note in Figure 7 that the flow velocities near the walls and baffles are high, so we have a turbulent flow in these areas, this explains why the boundary layer is thicker and more agitated, but the mixing is more efficient, which affects the transfer of momentum, heat and mass.
Turbulence is caused by excess kinetic energy in certain regions of the fluid flow, this excess energy counteracting the dissipation effect caused by the viscosity of the fluid. Thus, turbulence develops more easily in low viscosity fluids, and vice versa. In our analysis, the flow in solar heaters is irregular because the magnitudes of the Reynolds number larger than ($R_e$ = 10,000). Turbulence in a flow can be predicted from the Reynolds number, a dimensionless quantity that expresses the relationship through a power mobility of particles and the viscous dissipation in a given flow. Due to its complexity, turbulence has long eluded precise physical analysis. The interactions within turbulence make this phenomenon extremely complex, which is why we used the $k - \varepsilon$ in our study.

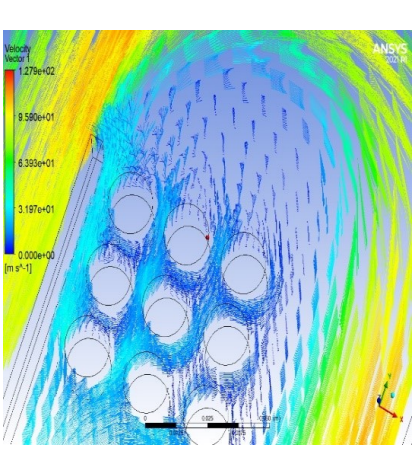

(A)

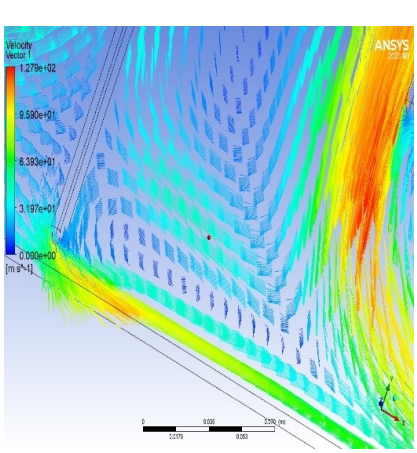

(A)

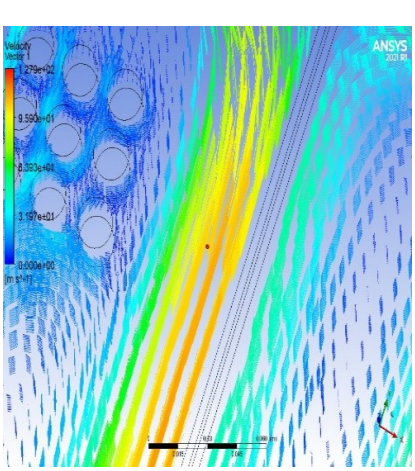

(A)

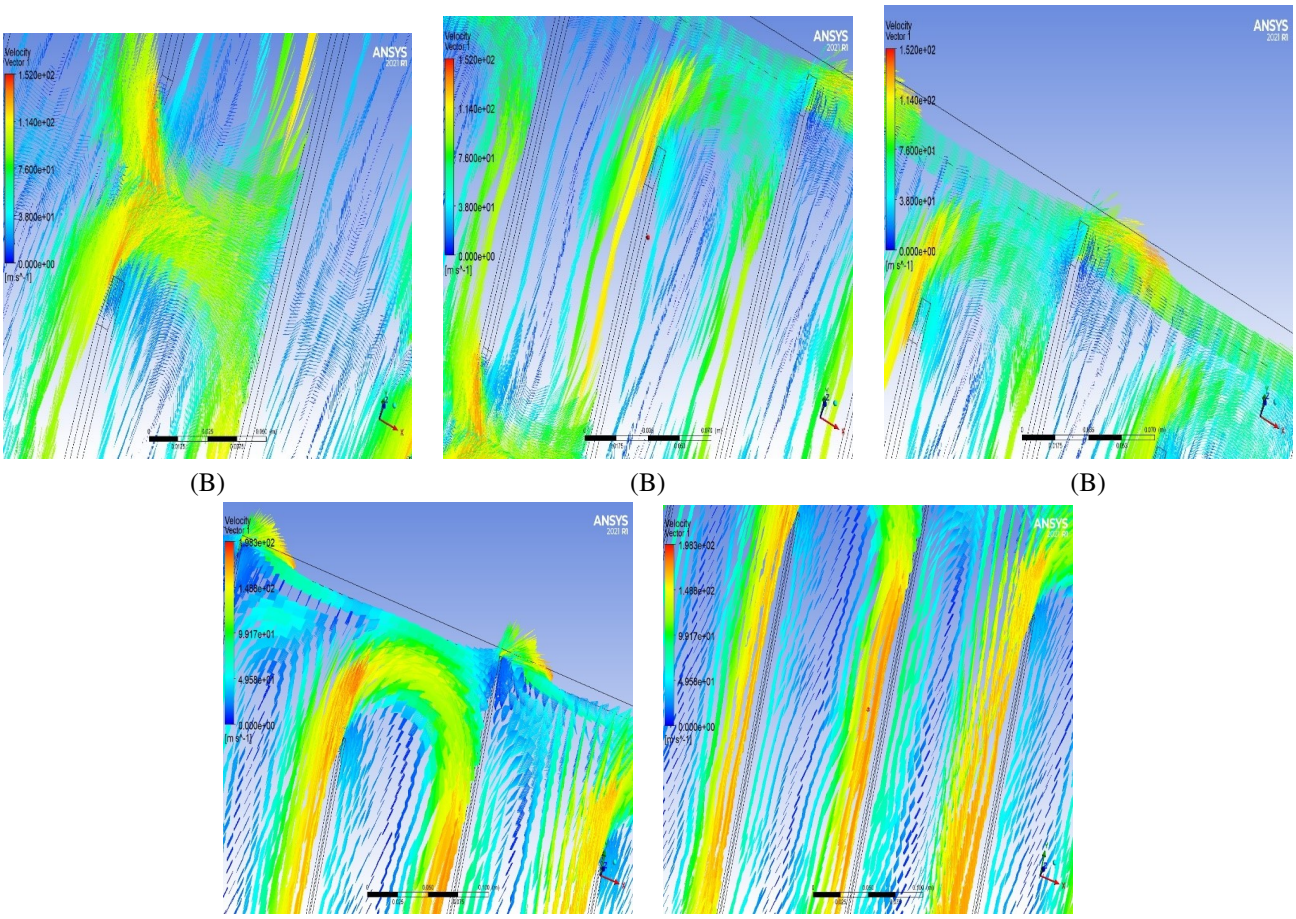


Fig. 7: Speed near walls and chicanes in model (SCTBSC) (A), model (SCDLTB) (B) and model (SCTB) (C) for : $V_e = 12m/s$

As illustrated in Figures 6 and 7, the division of $(k - \varepsilon)$ is very pronounced near the laterals of the collectors and obstacles, due to the reduction of the passage and the appearance of turbulent zones, a phenomenon observed in all the s collectors studied we have the magnitudes of $(k)$ for the type (SCTBSC) is 40.36 $m^2/s^2$, (SCDLTB) is 65.70 $m^2/s^2$ , (SCTB) is 137.4 $m^2/s^2$. the $k$ values for (SCDLTB) and (SCTB) are larger by 62.78% and 240.43%, respectively, compared to the (SCTBSC) model. Concerning the turbulent dissipation $(\varepsilon)$, it reached values of 1,938,000.02 $m^2/s^3$, 4,361,000.02 $m^2/s^3$ and 15,700,000.02 $m^2/s^3$ for the models (SCTBSC), (SCDLTB) and (SCTB), respectively. Significant magnitudes of $(\varepsilon)$ are presented in the models (SCDLTB) and (SCTB) amounting to 125.02% and 710.11%, respectively. Compared to the initial model (SCTBSC).

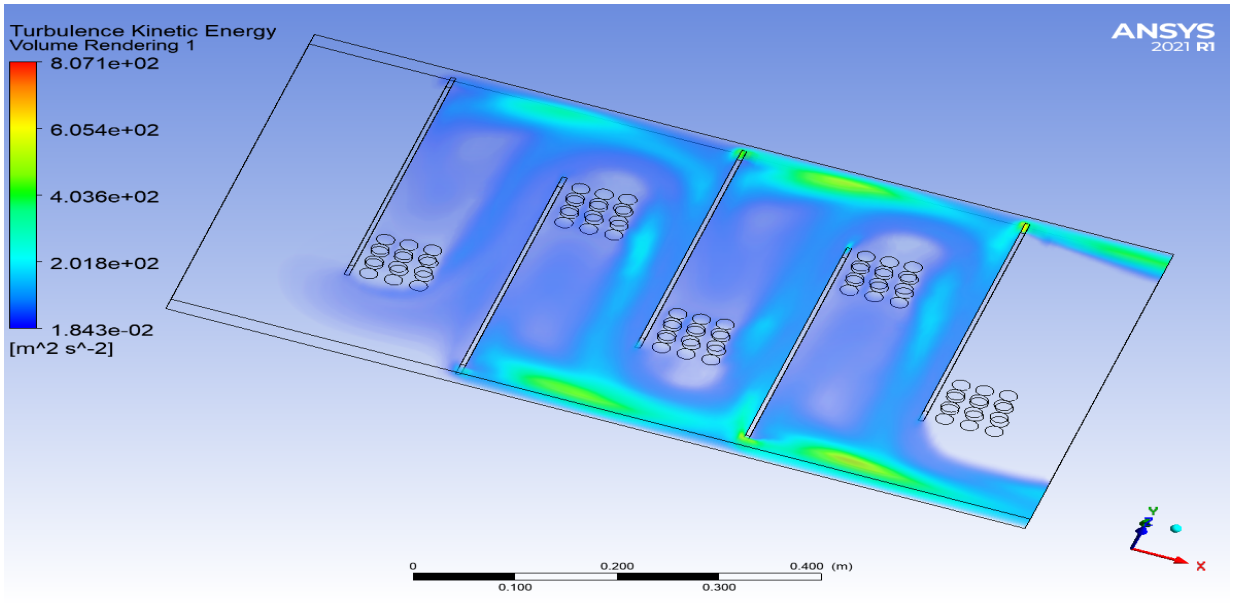


(A)

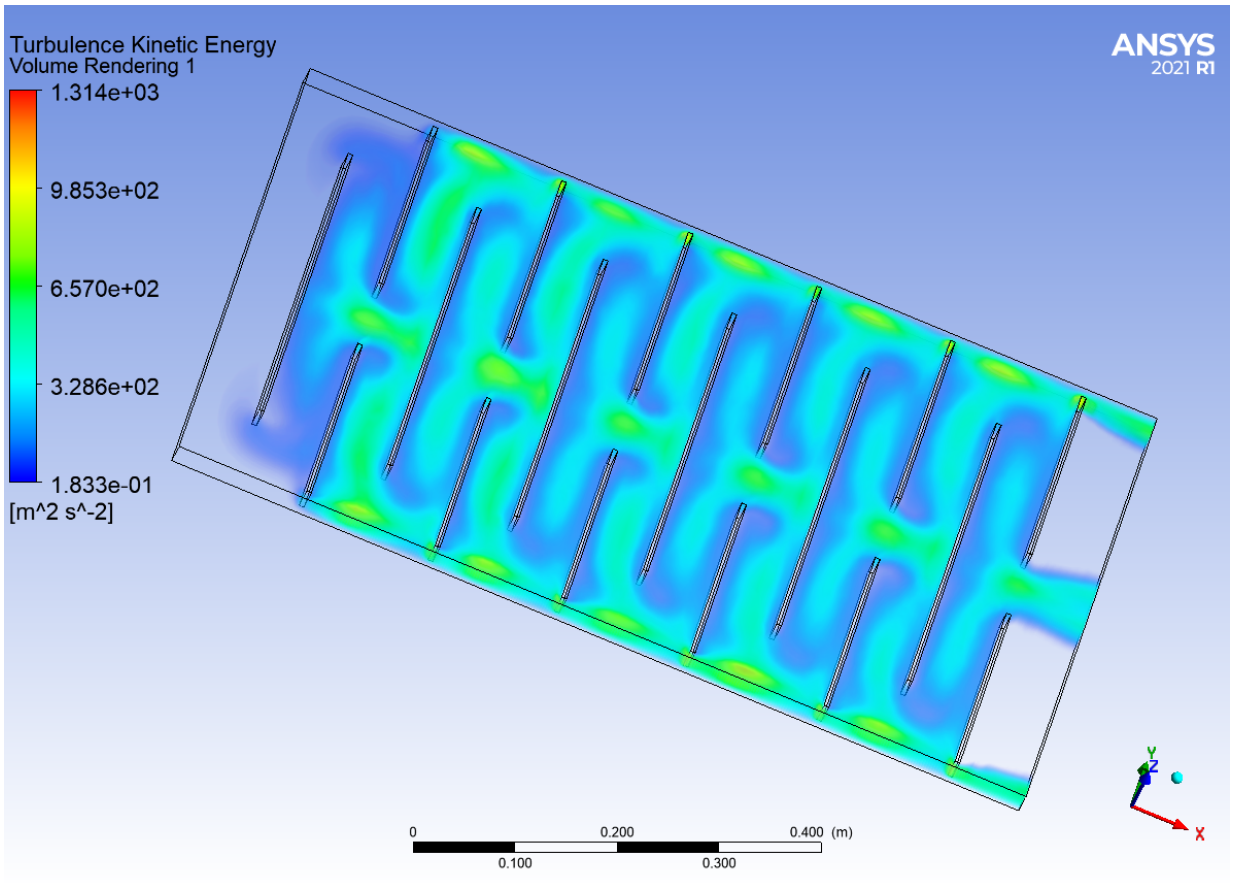


(B)

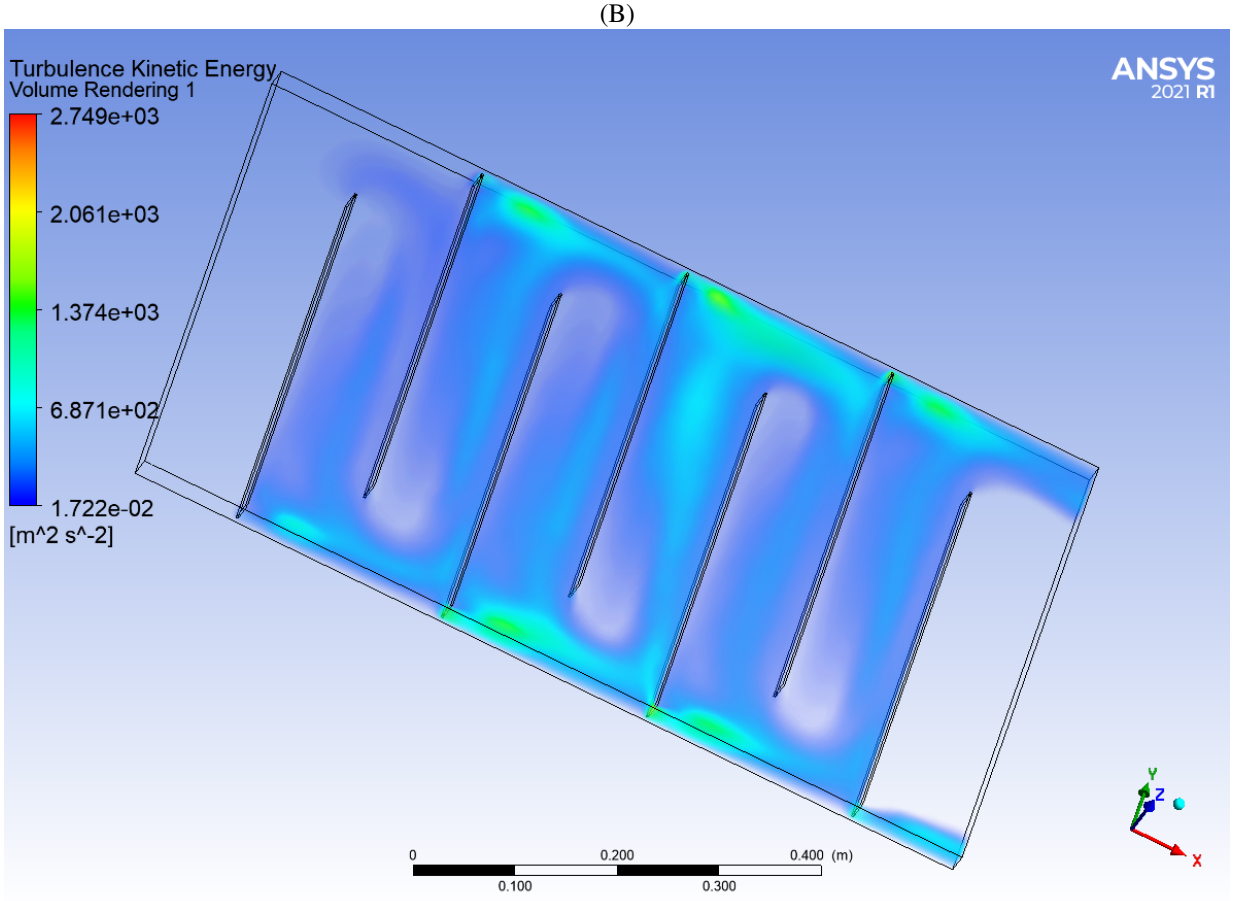


(C)

Fig. 8: Presentation of (k) in type (SCTBSC) (A), type (SCDLTB) (B) and type (SCTB) (C) for : $V_e = 12m/s$

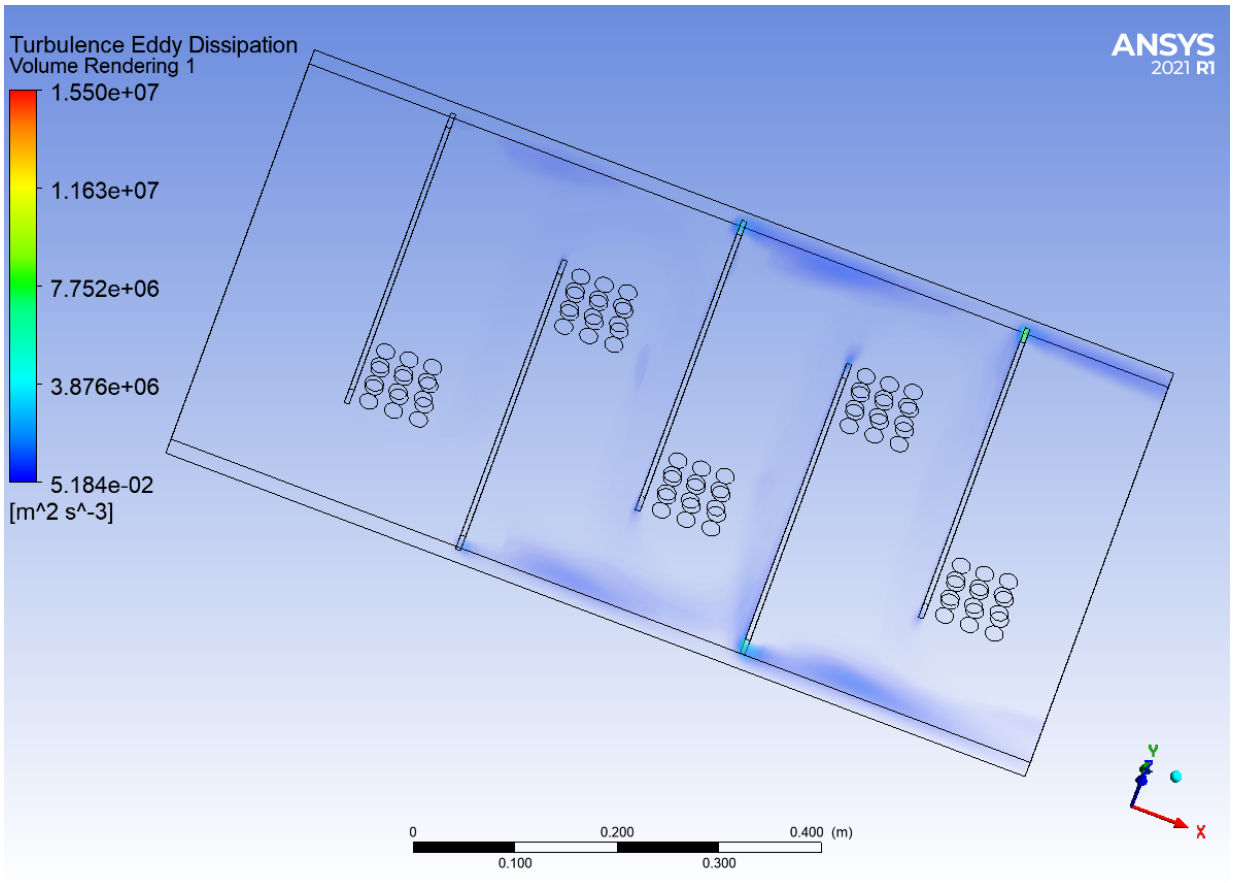
Turbulence Eddy Dissipation
Volume Rendering 1
1.550e+07
1.163e+07
7.752e+06
3.876e+06
5.184e-02
[m^2 s^-3]
ANSYS
2021 R1
0
0.200
0.400 (m)
0.100
0.300
Y
Z
X

(A)

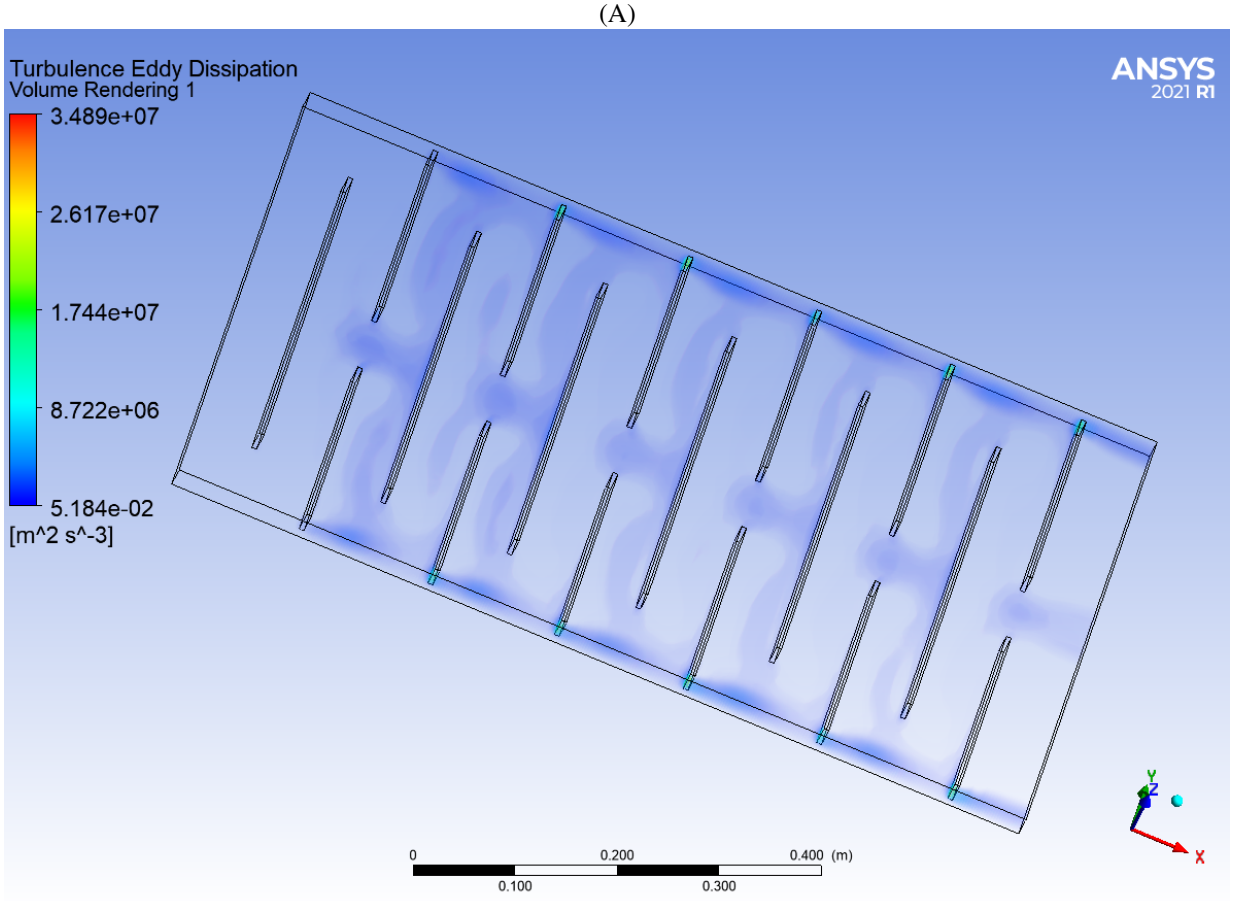
Turbulence Eddy Dissipation
Volume Rendering 1
3.489e+07
2.617e+07
1.744e+07
8.722e+06
5.184e-02
[m^2 s^-3]
ANSYS
2021 R1
0
0.200
0.400 (m)
0.100
0.300
Y
Z
X

(B)

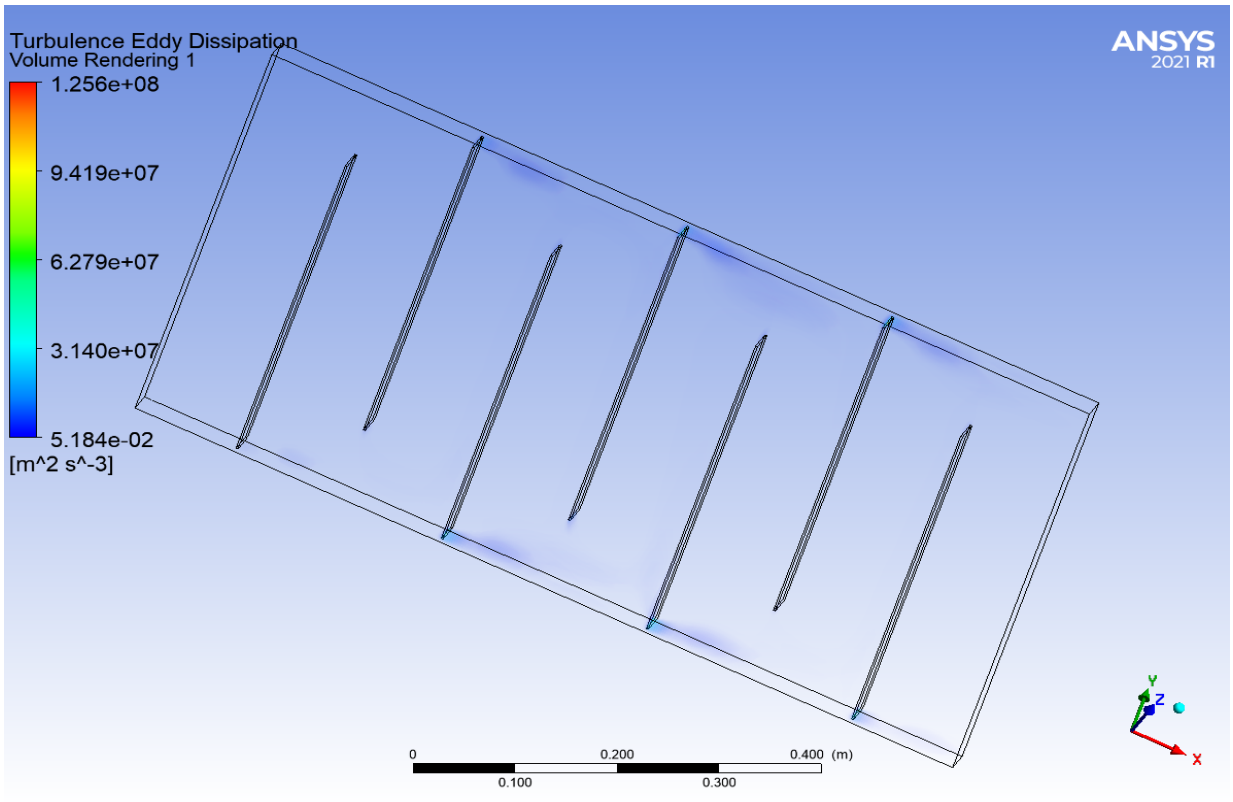


(C)

Fig. 9: Presentation of ($\varepsilon$) in type (SCTBSC) (A), type (SCDLTB) (B) and type (SCTB) (C) for : $V_e = 12m/s$

Heat transfer often involves ambiguities and confusion, particularly with temperature. While it is true that spontaneous heat transfers take place from places with warm temperatures to places with cold temperatures, it is nevertheless possible to achieve energy change from a cold body to a hot body like our collector models. Studied, the heat transmitted from the plate to the heat transfer fluid. We created turbulence using baffles to increase the collector quality.

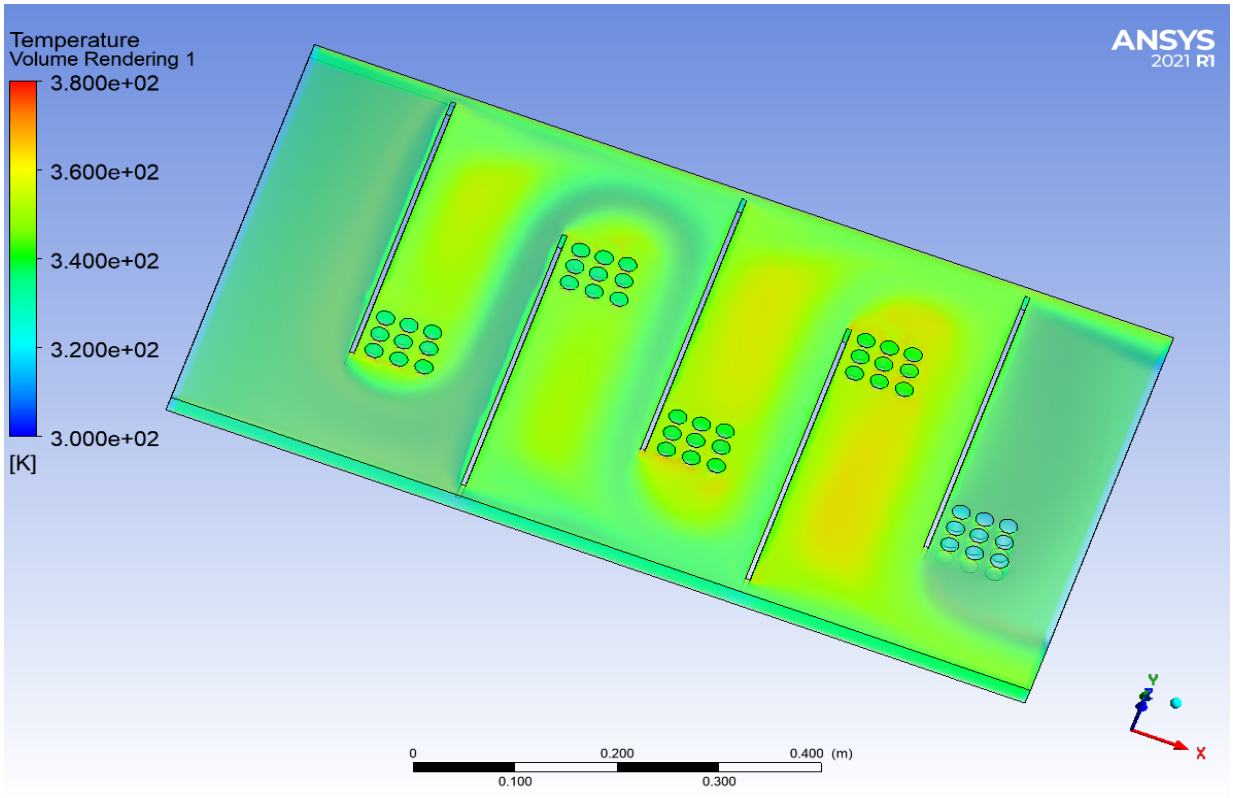


(A)

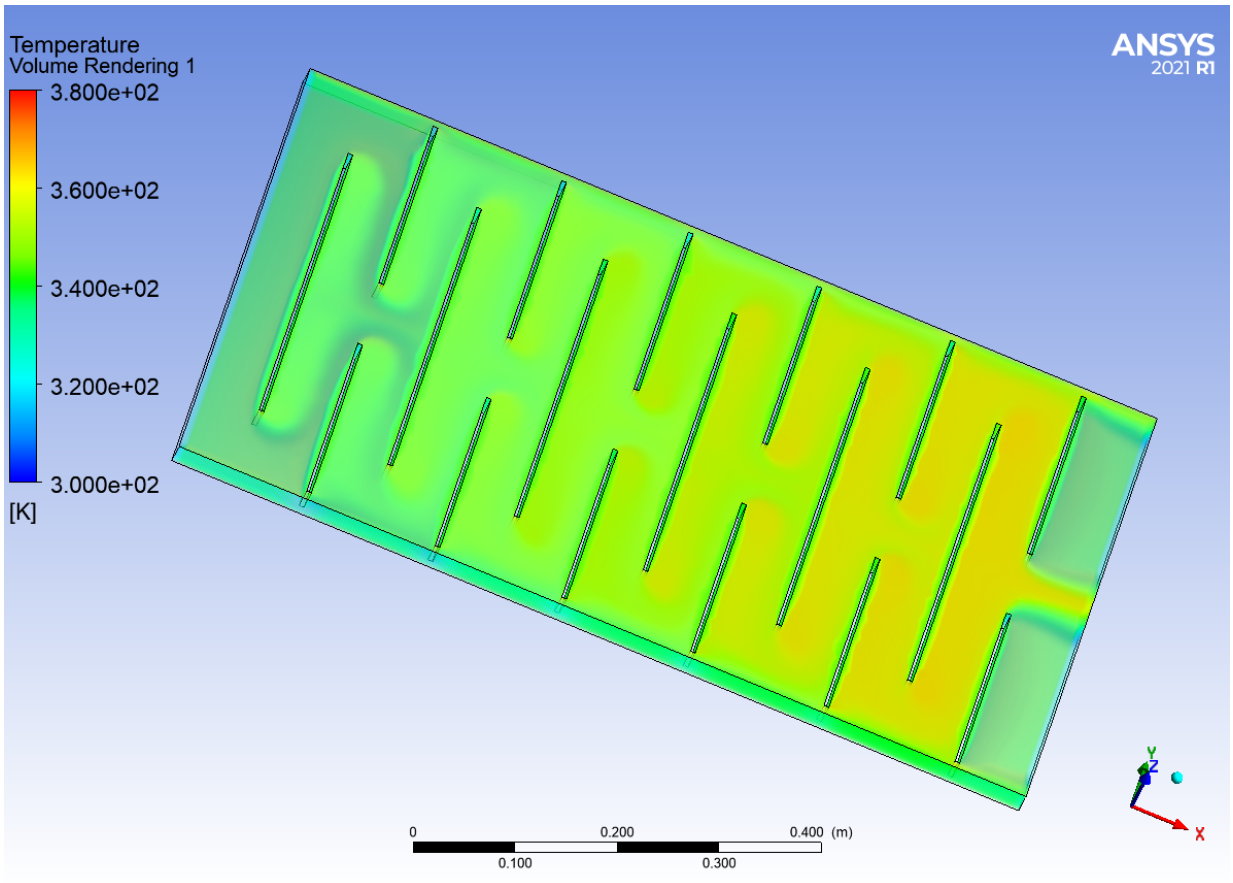


(B)

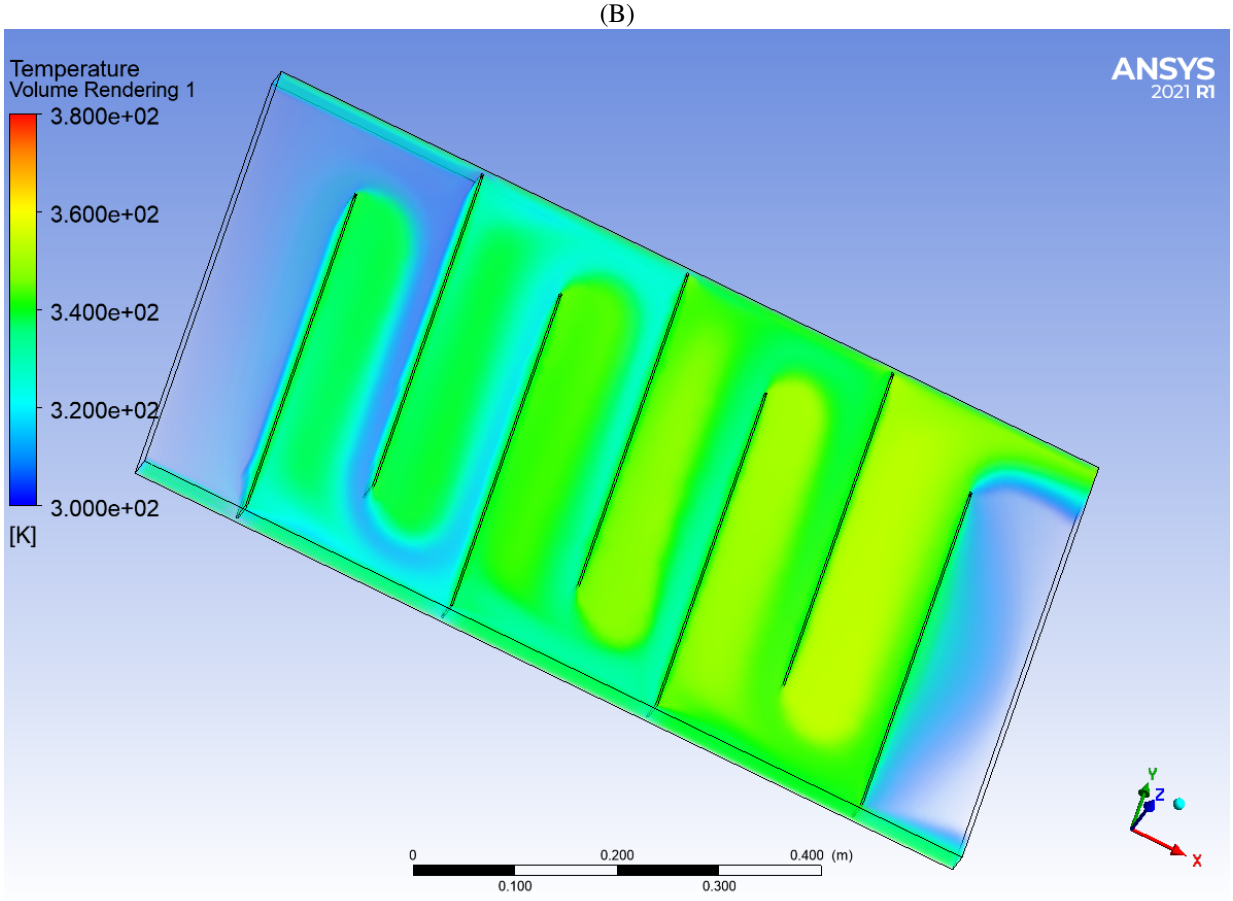


(C)

Fig. 10: Presentation of the temperature in model (SCTBSC) (A), model (SCDLTB) (B) and (SCTB) (C) for : $V_e = 12m/s$

The Nusselt number represents the intensity of thermal change, a dimensionless number representing the ratio of the effective heat flow to what it would be in pure conduction. Its value is therefore at least 1 (conduction only). Values close to 1 are representative

of laminar fluid flow, while values of 100 to 1000 can be obtained in turbulent flow. Dittus-Boelter determined the dimensionless local Nusselt number by:

$$Nu = 0,023\ Re^{4/5} Pr^{0.4} \tag{17}$$

where, $Re \geq 10^4$.

Graph 9 shows for a range of 60000 to 200000 (dimensionless Reynolds number) of the average Nusselt number (Nu) as a function of the Reynolds number, the flow velocity is set at 12 m/s then 15 m/s, the third is set at 18 m/s then at 21 m/s, the fifth at 24 m/s, increasing thereafter to 27 m/s and the last velocity is 30 m/s. To make a deeper analysis, we note that each velocity corresponds to Re and Nu and we observed that there is a relationship between the velocity, Re and Nu.

(Nu) for the model (SCTBSC) is 137 for an initial entry velocity of 12 m/s. when the admission speed increases, an increase in (Nu) is observed relative to the initial entry velocity, with respective increases of 17.51%, 38.68%, 57.66%, 74.45%, 89.05% and 105.84%.

We observe that (Nu) of the type (SCDLTB) take the value of 160 at an input speed of 12 m/s. when the admission speed increases, we notice an increase in the Nusselt number relative to this initial speed, with successive increases of 20%, 38.75%, 57.5%, 75%, 92.5% and 110%.

The model (SCTB) gives a Nusselt number of 164 for the first entry velocity of 12 m/s. when the admission speed increases, we notice an increase in the Nu in comparison with this starting vspeed, with increases of 20.12%, 39.63%, 58.53%, 76.82%, 94.51% and 112.19%.

For the first simulation, an inlet velocity of 12 m/s was set for the three models studied. We notice that the Nu for the (SCTBSC) type is 137. For this same inlet velocity, the (SCDLTB) and (SCTB) types show higher Nusselt numbers than those of the (SCTBSC) model, with respective deviations of 16.78% and 19.70%. For the other velocities, the deviations are (19.25%, 22.36%), (16.84%, 20.52%), (16.66%, 20.37%), (17.15%, 21.33%), (18.91%, 23.16%) and (19.14%, 23.40%), respectively.

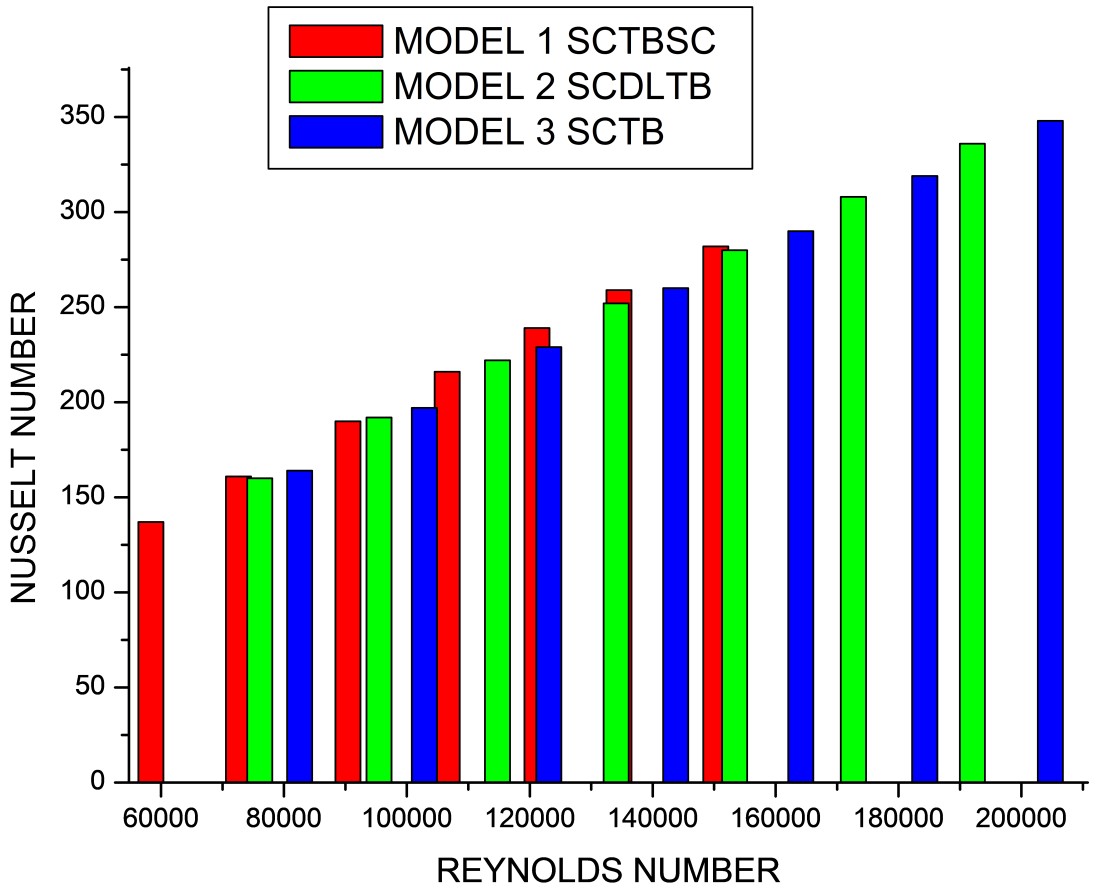


Fig. 11: The dimensionless number of Nu as a function of the dimensionless number of Re for the (SCTBSC) model (A), the (SCDLTB) model (B) and (SCTB) model (C)

The friction factor expressing the load loss or pressure loss during airflow within the fluid vein of the studied solar collectors. It is a dimensionless number, so its value is the same regardless of the unit system used for the other variables. The friction factor can also be called linear pressure loss coefficient which should not be confused with singular pressure loss coefficients. Petukhov established a correlation for smooth surfaces, covering different magnitudes of Re and it is expressed by $f$.

$$f = (0,79lnRE_D - 1,64)^{-2} \tag{18}$$

when the magnitude Re is in the middle of 3000 and $5 \times 10^6$, graph 10 shows a curve illustrating the reduction in $f$ as Re increases.

The value of $f$ of the type (SCTBSC) is 0,01993216 for a speed of 12 m/s, when the admission speed increases, we observe a decrease in $f$ compared to this initial velocity of respectively 4.43%, 8.63%, 11.63%, 13.89%, 15.66% and 17.49%.

In addition, $f$ of the type (SCDLTB) reaches 0,01908305 for a speed of 12 m/s. When the intake speed increases, a decrease in $f$ is observed relative to the intake speed, with decreases of 4.78%, 8.40%, 11.31%, 13.71%, 15.75% and 17.51%, respectively.

The magnitude of $f$ of the type (SCTB) is 0,01895342 regarding the speed of 12 m/s. When the intake speed increases, the $f$ decreases relative to the first intake speed by 4.82%, 8.47%, 11.45%, 13.86%, 15.89% and 17.66%, respectively.

We performed a computer simulation with an inlet velocity of 12 m/s for the three studied types. We found that the $f$ for the (SCTBSC) type reaches up to 0,01993216, while for the (SCDLTB) and (SCTB) models, the friction coefficients are 4.26% and 4.91% lower than the (SCTBSC) model, respectively. For the other velocities, the differences are (4.61% and 5.29%), (4.01% and 4.74%), (3.90% and 4.71%), (4.05% and 4.88%), (4.35% and 5.16%) and (4.28% and 5.10%), respectively.

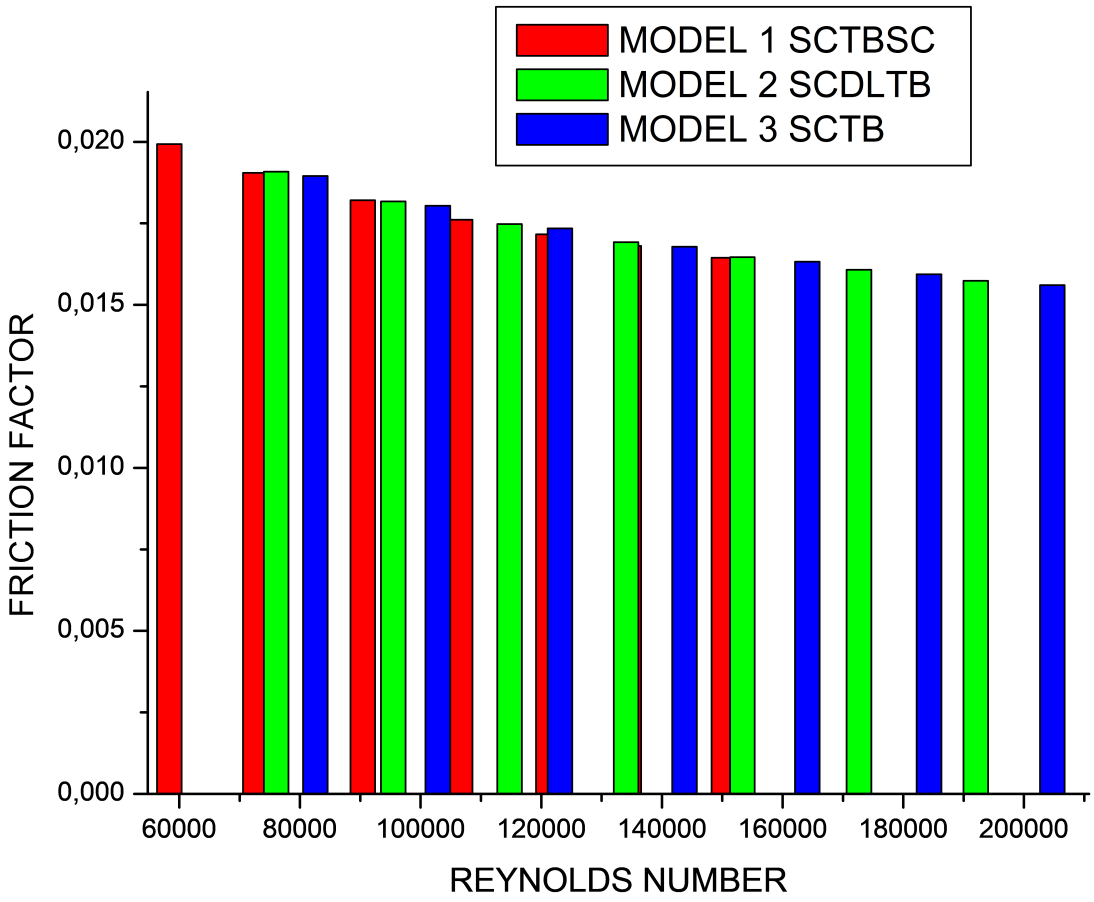


Fig. 12: The presentation of $f$ as a function Re for the model (SCTBSC) (A), model (SCDLTB) (B) and model (SCTB) (C)

Figure 11 presents a dimensionless number, called the Stanton number, which is employed in heat and mass exchange processes. This number is the relation of the bulk energy and the convective energy change in the studied solar air heaters, as also shown in graph 11. From Pr ≈ 1, the equation derived of the relationship for turbulent heat exchange in unobstruct ed tubes is relatively restricted. For the solution of plane surfaces, the analogy between energy change, displacementand friction, which relates fluid friction to heat transfer, has shown a use of Pr on $Pr^{2/3}$ and, consequently, on the Stanton number. For unsteady flow in tubes, this

use is adequate. The appropriate formula is used to calculate Pr:

$$St \cdot \ Pr^{2/3} = \frac{f}{8} \tag{19}$$

We find that with increasing $R_e$, the $P_r$ decreases, which is true for all four types studied (SCTBSC), (SCDLTB), and (SCTB).

For model (SCTBSC), the Stanton number is 0,00316556 at an inlet velocity of 12 m/s. When the intake speed increases, we observe a decrease in the Pr compared to the intake speed, with variations of 4.43%, 8.64%, 11.64%, 13.90%, 15.68%, and 17.51%, respectively.

Regarding the model (SCDLTB), the Stanton number reaches 0,00303194 at 12 m/s, and by increasing the intake speed, we also note a reduction in the Stanton number compared to the intake speed, with decreases of 4.78%, 8.41%, 11.31%, 13.72%, 15.76% and 17.53%, respectively.

We find that the Stanton number for the (SCTB) model is 0,00301293 at an inlet velocity of 12 m/s. When the intake speed increases, there is a decrease in the Pr compared to the intake speed, with decreases of 4.83%, 8.49%, 11.47%, 13.89%, 15.92%, and 17.69%, respectively.

We performed a computer simulation with an inlet velocity of 12 m/s for the three types studied. We noted that the Pr for the (SCTBSC) type reaches 0,00316556. For the (SCDLTB) and (SCTB) models, the Stanton numbers are lower than that of the (SCTBSC) model by 4.22% and 4.82%, respectively. For the other speeds, the observed differences are (4.57% and 5.21%), (3.97% and 4.66%), (3.86% and 4.63%), (4.01 and 4.80%), (4.30% and 5.08%) and (4.23% and 5.03%), respectively.

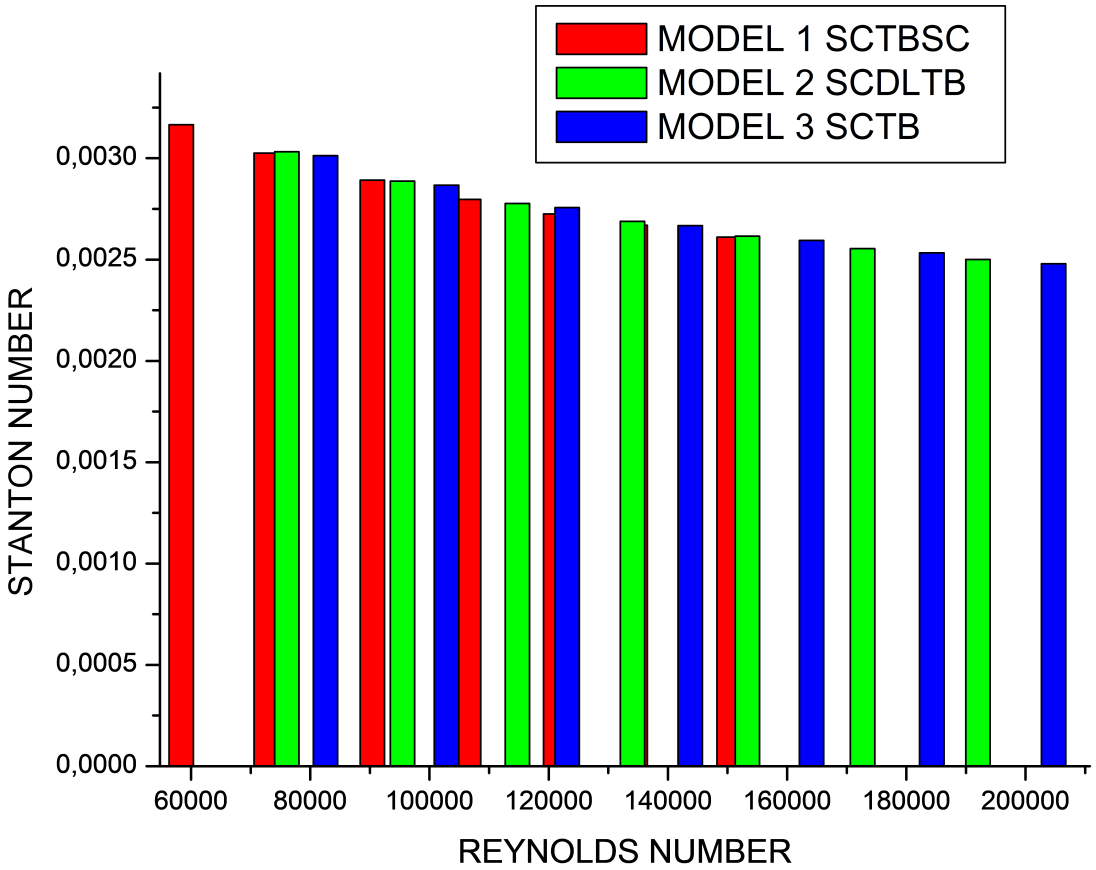


Fig. 13: The Stanton number as a function of the Reynolds number for the model (SCTBSC) (A), model (SCDLTB) (B) and model (SCTB) (C).

## 5 Conclusion

In our study, we numerically investigated, using computer software (CFD), three models of flat solar air heaters with different quality obstacles: the collector with transverse obstacles and small circular baffle (SCTBSC), the solar collector with different

lengths of transverse baffles (SCDLTB) and the solar collector with transverse baffles (SCTB). The aim was to analyze the aerodynamic and thermal flows in these solar s collectors. Several results were drawn regarding the aerodynamic characteristic:

- For the first model, with transverse baffles to extend the flow path in order to increase the exchange surface, as well as small circular baffles to eliminate the dead zones generated by the transverse baffles, the velocity around the baffles increased up to 832% compared to the inlet velocity.
- In the second model, we used a flat air solar collector with transverse baffles of different lengths, arranged to create a double passage in order to lengthen the flow path. We observed that the velocity at the exit of the baffles is very high, reaching up to 850% of the inlet velocity.
- The third model, which incorporates transverse baffles, also promotes an increase in air velocity and heat transfer. It was noted that the velocity near the baffles can reach 1552% compared to the inlet velocity.
- we have the magnitudes of (k) for the type (SCTBSC) is 40.36 $m^2/s^2$, (SCDLTB) is 65.70 $m^2/s^2$ , (SCTB) is 137.4 $m^2/s^2$. the k values for (SCDLTB) and (SCTB) are larger by 62.78% and 240.43%, respectively, compared to the (SCTBSC) model.
- Concerning the turbulent dissipation ($\varepsilon$), it reached values of 1,938,000.02 $m^2/s^3$, 4,361,000.02 $m^2/s^3$ and 15,700,000.02 $m^2/s^3$ for the models (SCTBSC), (SCDLTB) and (SCTB), respectively. Significant magnitudes of ($\varepsilon$) are presented in the models (SCDLTB) and (SCTB) amounting to 125.02% and 710.11%, respectively. Compared to the initial model (SCTBSC).
- For the first simulation, an inlet velocity of 12 m/s was set for the three models studied. We notice that the Nu for the (SCTBSC) type is 137. For this same inlet velocity, the (SCDLTB) and (SCTB) types show higher Nusselt numbers than those of the (SCTBSC) model, with respective deviations of 16.78% and 19.70%. For the other velocities, the deviations are (19.25%, 22.36%), (16.84%, 20.52%), (16.66%, 20.37%), (17.15%, 21.33%), (18.91%, 23.16%) and (19.14%, 23.40%), respectively.
- We performed a computer simulation with an inlet velocity of 12 m/s for the three studied types. We found that the f for the (SCTBSC) type reaches up to 0.01993216, while for the (SCDLTB) and (SCTB) models, the friction coefficients are 4.26% and 4.91% lower than the (SCTBSC) model, respectively. For the other velocities, the differences are (4.61% and 5.29%), (4.01% and 4.74%), (3.90% and 4.71%), (4.05% and 4.88%), (4.35% and 5.16%) and (4.28% and 5.10%), respectively.
- We performed a computer simulation with an inlet velocity of 12 m/s for the three types studied. We noted that the Pr for the (SCTBSC) type reaches 0.00316556. For the (SCDLTB) and (SCTB) models, the Stanton numbers are lower than that of the (SCTBSC) model by 4.22% and 4.82%, respectively. For the other speeds, the observed differences are (4.57% and 5.21%), (3.97% and 4.66%), (3.86% and 4.63%), (4.01 and 4.80%), (4.30% and 5.08%) and (4.23% and 5.03%), respectively.

## References


M. Abdelhafid. *Global and Local Study of the role of geometry in optimizing solar air flat plate collectors*. PhD thesis, University of Valenciennes and Hainaut Cambresis France, 1994.

G. Abdi, M. A. Amraoui, N. Medjadji, G. Lorenzini, and Y. Menni. 3d evaluation of a thermal and hydraulic winged solar collector. *Instrumentation Mesure Métrologie*, 21(2):35–41, 2022. doi: 10.18280/i2m.210201.

K. Aliane and M. A. Amraoui. Numerical study of a plane air solar collector having a rectangular roughness. *Renewable Energy Review*, 16(1):129–141, 2013. doi: 10.54966/jreen.v16i1.369.

M. A. Amraoui. *Numerical study of a flat air solar collector Influence of the shape of the roughness*. PhD thesis, Magister's Dissertation in mechanical engineering, 2011.

M. A. Amraoui. Three-dimensional numerical simulation of a flat plate solar collector with double paths. *International Journal of Heat and Technology*, 39(4):1087–1096, 2021a. doi: 10.18280/ijht.390406.

M. A. Amraoui. Numerical study of an air flow in a flat plate air solar collector with circular obstacles. In *Springer Nature Switzerland*, volume 174, pages 1–8, 2021b. doi: 10.1007/978-3-030-63846-7_81.

M. A. Amraoui and K. Aliane. Numerical analysis of a three dimensional fluid flow in a flat plate solar collector. *International Journal of Renewable and Sustainable Energy*, 3(3):68–75, 2014a. doi: 10.11648/j.ijrse.20140303.14.

M. A. Amraoui and K. Aliane. Dynamic and thermal study of the three-dimensional flow in a flat plate solar collector with transversal baffles. *International Review of Mechanical Engineering*, 8(5), 2014b. ISSN 1970-8734.

M. A. Amraoui and K. Aliane. Numerical study of the three-dimensional flow in a flat plate solar collector with baffles. In *22nd French Mechanics Congress*, 2015. URL https://hal.science/hal-03444952.

M. A. Amraoui and K. Aliane. Three-dimensional analysis of air flow in a flat plate solar collector. *Periodica Polytechnica Mechanical Engineering*, 62(2):126–135, 2018. doi: 10.3311/PPme.11255.

M. A. Amraoui and F. Benosman. Numerical modeling of a flat air solar collector fitted with obstacles. In *E3S Web of Conferences*, 2021. doi: 10.1051/e3sconf/202132104016.

M. A. Amraoui, M. A. Alkhafaji, S. Abdullaev, S. A. Zearah, A. Akgul, R. Jarrar, H. Shanak, J. Asad, and Y. Menni. CFD study of a dual-passage solar collector with longitudinal and transverse baffles for enhanced thermal performance. *Thermal science*, pages 3133–3142, 2023. doi: 10.2298/TSCI2304133A.

K. Aoues, N. Moummi, M. Zellouf, A. Moummi, A. Labed, E. Achouri, and A. Benchabane. Improvement of the thermal performance of a flat air solar collector: Experimental study in the biskra region. *Renewable Energy Review*, 12(2):237–248, 2009. doi: 10.54966/jreen.v12i2.135.

S. Bahria and M. Amirat. Influence of the addition of longitudinal baffles on the performance of an air-plane solar collector. *Renewable Energy Review*, 16(1), 2013. doi: 10.54966/jreen.v16i1.363.

A. Benkhelifa. Optimization of a planar solar collector. *Renewable Energy Review*, pages 13–18, 1998.

F. Benosman and M. A. Amraoui. Study of air flow in a solar collector equipped with two inclined obstacles. In *E3S Web of Conferences*, 2021. doi: 10.1051/e3sconf/202132104015.

L. Bourdeau, A. Jaffrin, and A. Moisan. Capture and storage of solar energy in homes using latent heat diode walls. *Journal de Physique Appliquée*, 15(3):559–568, 1980. doi: 10.1051/rphysap:01980001503055900.

M. T. Bouzaher, M. T. Baissi, and C. abdelbasset. Cfd analysis of solar air collector equipped with flexible ribs. *Journal of the Brazilian Society of Mechanical Sciences and Engineering*, 2019. doi: 10.1007/s40430-016-0500-3.

M. Cagnoli, L. Savoldi, R. Zanino, and F. Zaversky. Coupled optical and cfd parametric analysis of an open volumetric air receiver of honeycomb type for central tower CSP plants. *Solar Energy*, 155:523–536, 2017. doi: 10.1016/j.solener.2017.06.038.

G. Diarce, A. Campos-Celador, K. Martin, A. Urresti, A. García-Romero, and J. M. Sala. A comparative study of the CFD modeling of a ventilated active façade including phase change materials. *Applied Energy*, 126:307–317, 2014. doi: 10.1016/j.apenergy.2014.03.080.

M. A. Karim and Z. M. Amin. Mathematical modelling and performance analysis of different solar air collectors. *IIUM Engineering Journal*, pages 43–55, 2015. doi: 10.31436/iiumej.v16i2.603.

S. Khaldi, A. N. Korti, and S. Abboudi. Improving the airflow distribution within an indirect solar dryer by modifications based on computational fluid dynamics. *International Journal of Air-Conditioning and Refrigeration*, 25(3), 2017a. doi: 10.1142/S2010132517500225.

S. Khaldi, N. Korti, and S. Abboudi. Applying CFD for studying the dynamic and thermal behavior of solar chimney drying system with reversed absorber. *International Journal of Food Engineering*, 13(9), 2017b. doi: 10.1515/ijfe-2017-0081.

Y. Menni, A. Azzi, and A. Chamkha. Enhancement of convective heat transfer in smooth air channels with wall-mounted obstacles in the flow path. *Journal of Thermal Analysis and Calorimetry*, 135:1951–1976, 2019a. doi: 10.1007/s10973-018-7268-x.

Y. Menni, A. Azzi, A. Chamkha, and S. Harmand. Analysis of fluid dynamics and heat transfer in a rectangular duct with staggered baffles. *Journal of Applied and Computational Mechanics*, 5(2):231–248, 2019b. doi: 10.22055/JACM.2018.26023.1305.

Y. Menni, H. Ameur, S. Yao, M. A. Amraoui, M. Inc, G. Lorenzini, and H. Ahmad. Computational fluid dynamic simulations and heat transfer characteristic comparisons of various arc-baffled channels. *Open Physics*, 19:51–60, 2021. doi: 10.1515/phys-2021-0005.

F. Mokhtari and D. Semmar. Experimental study of a solar air collector. *Renewable Energy Review*, pages 243–246, 1999.

D. Semmar, S. Betrouni, and D. Lafri. Study and creation of a solar air collector. *Renewable Energy Review*, pages 33–38, 1998.

R. Ben Slama. The air solar collectors: Comparative study, introduction of baffles to favor the heat transfer. *Solar Energy*, 81(2): 139–149, 2007. doi: 10.1016/j.solener.2006.05.002.

G. Villi, W. Pasut, and M. De Carli. CFD modelling and thermal performance analysis of a wooden ventilated roof structure. *Building Simulation*, 2:215–228, 2009. doi: 10.1007/s12273-009-9414-7.

D. C. Wilcox. *Turbulence Modeling for CFD*. DCW Industries, La Cañada, USA, 1993.

A. Zerrouki, B. Tedjiza, and N. Said. Modeling thermal losses in a two-pass air solar collector. *Renewable Energy Review*, 5: 49–58, 2002.

C. Zilio, G. A. Longo, G. Pernigotto, F. Chiacchio, P. Borrelli, and E. D'Errico. CFD analysis of aircraft fuel tanks thermal behavior. In *IOP Conference Series: Journal of Physics*, volume 923, 2017. doi: 10.1088/1742-6596/923/1/012027.